MEF2 pathway is used for insulin-like growth factor-induced myogenin expression (54). Huddleson *et al.* (42) have also shown that induction of KLF2 by shear stress requires a PI3K/chromatin-remodeling pathway. In contrast to our result, they claimed that AKT is not involved in this pathway, although it is activated by shear stress. We propose the involvement of AKT in Ang1-mediated KLF2 induction because 1) AKT inhibitor and knockdown of AKT both inhibit KLF2 mRNA and protein expression by COMP-Ang1; 2) AKT-CA induces the MEF2-dependent transcription and stimulates the KLF2 promoter cooperatively with MEF2; and 3) overexpression of AKT-CA induces both mRNA and protein expression of KLF2 in HUVECs. Currently, the reason for this discrepancy remains unclear, but it may be due to the different cell types used for the experiments. We performed the experiments with HUVECs, whereas they used an EOMA cell line. Alternatively, different stimuli such as Ang1 and shear stress may trigger distinct signaling pathways downstream of PI3K to stimulate KLF2 induction.

At present, a molecular link between AKT and MEF2 is still unknown. Recently, it has been reported that AKT directly phosphorylates transcriptional coactivator p300, leading to the association of MyoD with p300 and p300/CBP-associated factor (PCAF) (55). In addition, it has been also shown that p300 can physically interact with MEF2 as well as MyoD and enhances their transcriptional activity (28). Importantly, shear stress is shown to induce recruitment of p300 and PCAF into the KLF2 promoter (42). Therefore, the Ang1/Tie2/PI3K/AKT pathway may induce the association of MEF2 with transcriptional coactivators such as p300 and PCAF, thereby stimulating its transcriptional activity. p300 directly acetylates and stimulates MEF2 activity (51). However, PI3K-mediated activation of MEF2 is not mediated by such direct acetylation mechanism because transcriptional activity of acetylation-defective mutant of MEF2 could be stimulated by constitutive active PI3K (supplemental Fig. S3). Thus, further examination is required for clarifying the molecular link between AKT and MEF2.

KLF2 inhibits VEGF-induced angiogenesis and inflammation, possibly by maintaining vascular quiescence. Similarly, Ang1 counteracts VEGF-mediated inflammatory responses. Our present data suggest that inhibition of VEGF-mediated inflammatory responses by Ang1 depends upon KLF2. However, Ang1 also acts cooperatively with VEGF to induce angiogenesis in a certain situation (5, 7, 9). This opposite effect of Ang1 on VEGF-mediated responses may depend upon whether KLF2 is induced or not. In the presence of cell-cell contacts, Ang1/Tie2 signal is able to induce KLF2 expression and thereby inhibits VEGF-induced inflammation and angiogenesis. However, in the absence of cell-cell contacts, Ang1/Tie2 signal accelerates angiogenic signal because KLF2 is not induced in this condition, which accounts for the cooperation of Ang1 with VEGF. Therefore, KLF2 may be a key downstream factor from *trans*-associated Tie2 to maintain vascular quiescence.

In conclusion, we found that Ang1/Tie2 signal stimulates transcriptional activity of MEF2 through a PI3K/AKT pathway to induce KLF2 expression, thereby contributing to vascular quiescence.

Acknowledgments—We are grateful to M. K. Jain and G. B. Atkins (Case Western Reserve University) for the KLF2-Luc reporter plasmid, to Y. Fujio (Osaka University) for the adenovirus encoding AKT-CA, to C. Grozinger for the expression vector for HDAC5 (Harvard University), to K. Matsuo, M. Sone, M. Minamimoto, M. Maeoka, and Y. Matsuura for technical assistance, and to N. Takakura (Osaka University), M. Murakami (Kyoto University), H. Fujita (Osaka City University), and H. Daitoku (University of Tsukuba) for helpful advice.

REFERENCES

1. Dumont, D. J., Gradwohl, G., Fong, G. H., Puri, M. C., Gertsenstein, M., Auerbach, A., and Breitman, M. L. (1994) *Genes Dev.* **8,** 1897–1909
2. Suri, C., Jones, P. F., Patan, S., Bartunkova, S., Maisonpierre, P. C., Davis, S., Sato, T. N., and Yancopoulos, G. D. (1996) *Cell* **87,** 1171–1180
3. Sato, T. N., Tozawa, Y., Deutsch, U., Wolburg-Buchholz, K., Fujiwara, Y., Gendron-Maguire, M., Gridley, T., Wolburg, H., Risau, W., and Qin, Y. (1995) *Nature* **376,** 70–74
4. Wong, A. L., Haroon, Z. A., Werner, S., Dewhirst, M. W., Greenberg, C. S., and Peters, K. G. (1997) *Circ. Res.* **81,** 567–574
5. Peters, K. G., Kontos, C. D., Lin, P. C., Wong, A. L., Rao, P., Huang, L., Dewhirst, M. W., and Sankar, S. (2004) *Recent Prog. Horm. Res.* **59,** 51–71
6. Brindle, N. P., Saharinen, P., and Alitalo, K. (2006) *Circ. Res.* **98,** 1014–1023
7. Asahara, T., Chen, D., Takahashi, T., Fujikawa, K., Kearney, M., Magner, M., Yancopoulos, G. D., and Isner, J. M. (1998) *Circ. Res.* **83,** 233–240
8. Lin, P., Polverini, P., Dewhirst, M., Shan, S., Rao, P. S., and Peters, K. (1997) *J. Clin. Investig.* **100,** 2072–2078
9. Eklund, L., and Olsen, B. R. (2006) *Exp. Cell Res.* **312,** 630–641
10. Fukuhara, S., Sako, K., Minami, T., Noda, K., Kim, H. Z., Kodama, T., Shibuya, M., Takakura, N., Koh, G. Y., and Mochizuki, N. (2008) *Nat. Cell Biol.* **10,** 513–526
11. Saharinen, P., Eklund, L., Miettinen, J., Wirkkala, R., Anisimov, A., Winderlich, M., Nottebaum, A., Vestweber, D., Deutsch, U., Koh, G. Y., Olsen, B. R., and Alitalo, K. (2008) *Nat. Cell Biol.* **10,** 527–537
12. Kuo, C. T., Veselits, M. L., Barton, K. P., Lu, M. M., Clendenin, C., and Leiden, J. M. (1997) *Genes Dev.* **11,** 2996–3006
13. Lee, J. S., Yu, Q., Shin, J. T., Sebzda, E., Bertozzi, C., Chen, M., Mericko, P., Stadtfeld, M., Zhou, D., Cheng, L., Graf, T., MacRae, C. A., Lepore, J. J., Lo, C. W., and Kahn, M. L. (2006) *Dev. Cell* **11,** 845–857
14. Wu, J., Bohanan, C. S., Neumann, J. C., and Lingrel, J. B. (2008) *J. Biol. Chem.* **283,** 3942–3950
15. Atkins, G. B., and Jain, M. K. (2007) *Circ. Res.* **100,** 1686–1695
16. Dekker, R. J., van Soest, S., Fontijn, R. D., Salamanca, S., de Groot, P. G., VanBavel, E., Pannekoek, H., and Horrevoets, A. J. G. (2002) *Blood* **100,** 1689–1698
17. Huddleson, J. P., Srinivasan, S., Ahmad, N., and Lingrel, J. B. (2004) *Biol. Chem.* **385,** 723–729
18. Dekker, R. J., van Thienen, J. V., Rohlena, J., de Jager, S. C., Elderkamp, Y. W., Seppen, J., de Vries, C. J. M., Biessen, E. A. L., van Berkel, T. J. C., Pannekoek, H., and Horrevoets, A. J. G. (2005) *Am. J. Pathol.* **167,** 609–618
19. Parmar, K. M., Larman, H. B., Dai, G., Zhang, Y., Wang, E. T., Moorthy, S. N., Kratz, J. R., Lin, Z., Jain, M. K., Gimbrone, M. A., Jr., and Garcia-Cardena, G. (2006) *J. Clin. Investig.* **116,** 49–58
20. Kumar, A., Lin, Z., SenBanerjee, S., and Jain, M. K. (2005) *Mol. Cell. Biol.* **25,** 5893–5903
21. Hayashi, M., Kim, S. W., Imanaka-Yoshida, K., Yoshida, T., Abel, E. D., Eliceiri, B., Yang, Y., Ulevitch, R. J., and Lee, J. D. (2004) *J. Clin. Investig.* **113,** 1138–1148
22. Olson, E. N. (2004) *J. Clin. Investig.* **113,** 1110–1112
23. Wang, L., Fan, C., Topol, S. E., Topol, E. J., and Wang, Q. (2003) *Science* **302,** 1578–1581
24. SenBanerjee, S., Lin, Z., Atkins, G. B., Greif, D. M., Rao, R. M., Kumar, A., Feinberg, M. W., Chen, Z., Simon, D. I., Luscinskas, F. W., Michel, T. M., Gimbrone, M. A., Jr., Garcia-Cardena, G., and Jain, M. K. (2004) *J. Exp.*

Med. **199,** 1305–1315
25. Lin, Z., Hamik, A., Jain, R., Kumar, A., and Jain, M. K. (2006) *Arterioscler. Thromb. Vasc. Biol.* **26,** 1185–1189
26. Bhattacharya, R., SenBanerjee, S., Lin, Z., Mir, S., Hamik, A., Wang, P., Mukherjee, P., Mukhopadhyay, D., and Jain, M. K. (2005) *J. Biol. Chem.* **280,** 28848–28851
27. Dekker, R. J., Boon, R. A., Rondaij, M. G., Kragt, A., Volger, O. L., Elderkamp, Y. W., Meijers, J. C. M., Voorberg, J., Pannekoek, H., and Horrevoets, A. J. G. (2006) *Blood* **107,** 4354–4363
28. Sartorelli, V., Huang, J., Hamamori, Y., and Kedes, L. (1997) *Mol. Cell. Biol.* **17,** 1010–1026
29. Gamble, J. R., Drew, J., Trezise, L., Underwood, A., Parsons, M., Kasminkas, L., Rudge, J., Yancopoulos, G., and Vadas, M. A. (2000) *Circ. Res.* **87,** 603–607
30. Kim, I., Moon, S. O., Hoon Kim, S., Jin Kim, H., Soon Koh, Y., and Young Koh, G. (2001) *J. Biol. Chem.* **276,** 7614–7620
31. Gavard, J., Patel, V., and Gutkind, J. S. (2008) *Dev. Cell* **14,** 25–36
32. Thurston, G., Suri, C., Smith, K., McClain, J., Sato, T. N., Yancopoulos, G. D., and McDonald, D. M. (1999) *Science* **286,** 2511–2514
33. Thurston, G., Rudge, J. S., Ioffe, E., Zhou, H., Ross, L., Croll, S. D., Glazer, N., Holash, J., McDonald, D. M., and Yancopoulos, G. D. (2000) *Nat. Med.* **6,** 460–463
34. Cho, C. H., Kammerer, R. A., Lee, H. J., Steinmetz, M. O., Ryu, Y. S., Lee, S. H., Yasunaga, K., Kim, K. T., Kim, I., Choi, H. H., Kim, W., Kim, S. H., Park, S. K., Lee, G. M., and Koh, G. Y. (2004) *Proc. Natl. Acad. Sci. U. S. A.* **101,** 5547–5552
35. Sakurai, A., Fukuhara, S., Yamagishi, A., Sako, K., Kamioka, Y., Masuda, M., Nakaoka, Y., and Mochizuki, N. (2006) *Mol. Biol. Cell* **17,** 966–976
36. Marinissen, M. J., Chiariello, M., Pallante, M., and Gutkind, J. S. (1999) *Mol. Cell. Biol.* **19,** 4289–4301
37. Coso, O. A., Montaner, S., Fromm, C., Lacal, J. C., Prywes, R., Teramoto, H., and Gutkind, J. S. (1997) *J. Biol. Chem.* **272,** 20691–20697
38. Murga, C., Fukuhara, S., and Gutkind, J. S. (2000) *J. Biol. Chem.* **275,** 12069–12073
39. Fukuhara, S., Sakurai, A., Sano, H., Yamagishi, A., Somekawa, S., Takakura, N., Saito, Y., Kangawa, K., and Mochizuki, N. (2005) *Mol. Cell. Biol.* **25,** 136–146
40. Fukuhara, S., Marinissen, M. J., Chiariello, M., and Gutkind, J. S. (2000) *J. Biol. Chem.* **275,** 21730–21736
41. Sen-Banerjee, S., Mir, S., Lin, Z., Hamik, A., Atkins, G. B., Das, H., Banerjee, P., Kumar, A., and Jain, M. K. (2005) *Circulation* **112,** 720–726
42. Huddleson, J. P., Ahmad, N., Srinivasan, S., and Lingrel, J. B. (2005) *J. Biol. Chem.* **280,** 23371–23379
43. Kato, Y., Kravchenko, V. V., Tapping, R. I., Han, J., Ulevitch, R. J., and Lee, J. D. (1997) *EMBO J.* **16,** 7054–7066
44. Kato, Y., Zhao, M., Morikawa, A., Sugiyama, T., Chakravortty, D., Koide, N., Yoshida, T., Tapping, R. I., Yang, Y., Yokochi, T., and Lee, J. D. (2000) *J. Biol. Chem.* **275,** 18534–18540
45. Sohn, S. J., Li, D., Lee, L. K., and Winoto, A. (2005) *Mol. Cell. Biol.* **25,** 8553–8566
46. McKinsey, T. A., Zhang, C. L., and Olson, E. N. (2002) *Curr. Opin. Cell Biol.* **14,** 763–772
47. McKinsey, T. A., Zhang, C. L., Lu, J., and Olson, E. N. (2000) *Nature* **408,** 106–111
48. Vega, R. B., Harrison, B. C., Meadows, E., Roberts, C. R., Papst, P. J., Olson, E. N., and McKinsey, T. A. (2004) *Mol. Cell. Biol.* **24,** 8374–8385
49. Potthoff, M. J., and Olson, E. N. (2007) *Development (Camb.)* **134,** 4131–4140
50. Han, J., Jiang, Y., Li, Z., Kravchenko, V. V., and Ulevitch, R. J. (1997) *Nature* **386,** 296–299
51. Ma, K., Chan, J. K. L., Zhu, G., and Wu, Z. (2005) *Mol. Cell. Biol.* **25,** 3575–3582
52. Bi, W., Drake, C. J., and Schwarz, J. J. (1999) *Dev. Biol.* **211,** 255–267
53. Deng, Y., Yang, J., McCarty, M., and Su, B. (2007) *Am. J. Physiol.* **293,** C1404–C1411
54. Xu, Q., and Wu, Z. (2000) *J. Biol. Chem.* **275,** 36750–36757
55. Serra, C., Palacios, D., Mozzetta, C., Forcales, S. V., Morantte, I., Ripani, M., Jones, D. R., Du, K., Jhala, U. S., Simone, C., and Puri, P. L. (2007) *Mol. Cell* **28,** 200–213

Activation of Na^+/H^+ Exchanger 1 Is Sufficient to Generate Ca^{2+} Signals That Induce Cardiac Hypertrophy and Heart Failure

Tomoe Y. Nakamura,* Yuko Iwata,* Yuji Arai, Kazuo Komamura, Shigeo Wakabayashi

Abstract—Activation of the sarcolemmal Na^+/H^+ exchanger (NHE)1 is increasingly documented as a process involved in cardiac hypertrophy and heart failure. However, whether NHE1 activation alone is sufficient to induce such remodeling remains unknown. We generated transgenic mice that overexpress a human NHE1 with high activity in hearts. The hearts of these mice developed cardiac hypertrophy, contractile dysfunction, and heart failure. In isolated transgenic myocytes, intracellular pH was elevated in Hepes buffer but not in physiological bicarbonate buffer, yet intracellular Na^+ concentrations were higher under both conditions. In addition, both diastolic and systolic Ca^{2+} levels were increased as a consequence of Na^+-induced Ca^{2+} overload; this was accompanied by enhanced sarcoplasmic reticulum Ca^{2+} loading via Ca^{2+}/calmodulin-dependent protein kinase (CaMK)II-dependent phosphorylation of phospholamban. Negative force–frequency dependence was observed with preservation of high Ca^{2+}, suggesting a decrease in myofibril Ca^{2+} sensitivity. Furthermore, the Ca^{2+}-dependent prohypertrophic molecules calcineurin and CaMKII were highly activated in transgenic hearts. These effects observed in vivo and in vitro were largely prevented by the NHE1 inhibitor cariporide. Interestingly, overexpression of NHE1 in neonatal rat ventricular myocytes induced cariporide-sensitive nuclear translocation of NFAT (nuclear factor of activated T cells) and nuclear export of histone deacetylase 4, suggesting that increased Na^+/H^+ exchange activity can alter hypertrophy-associated gene expression. However, in transgenic myocytes, contrary to exclusive translocation of histone deacetylase 4, NFAT only partially translocated to nucleus, possibly because of marked activation of p38, a negative regulator of NFAT signaling. We conclude that activation of NHE1 is sufficient to initiate cardiac hypertrophy and heart failure mainly through activation of CaMKII–histone deacetylase pathway. (***Circ Res.* 2008;103:891-899.**)

Key Words: Na^+/H^+ exchanger ■ Na^+ and Ca^{2+} overload ■ cardiac remodeling ■ CaMKII-HDAC pathway ■ calcineurin–NFAT pathway

Intracellular Na^+ levels are regulated by a network of ion channels and transporters.[1] In the myocardium, Na^+ homeostasis is closely linked to intracellular Ca^{2+} handling via the Na^+/Ca^{2+} exchanger (NCX), the principal mechanism for Ca^{2+} efflux from cardiomyocytes. Na^+ dysfunction alters Ca^{2+} homeostasis, thereby contributing to the pathogenesis of heart failure (HF) in animal models and in humans. The sarcolemmal Na^+/H^+ exchanger (NHE)1 is a major Na^+ influx pathway that also serves as a powerful acid extrusion system. NHE1 couples H^+ efflux to Na^+ influx in a 1:1 stoichiometry under the driving force of a Na^+ gradient formed by the Na^+ pump. Thus, enhanced NHE activity leads to elevated intracellular Na^+ concentration ($[Na^+]_i$) and cytoplasmic alkalinization. NHE1 activity is controlled by intracellular pH (pH_i) and numerous other factors, such as hormones, catecholamines, and mechanical stimuli, known to be associated with a failing heart. NHE1 activity has been implicated in myocardial ischemia and reperfusion injury,[2] and NHE1 inhibition was reported to protect against these injuries in animal models and in patients undergoing coronary interventions.[3] However, in other cardiac disease states such as cardiac remodeling process, the role of NHE1 is not fully understood. It has been proposed that enhanced myocardial NHE1 activity is partially responsible for the cardiac remodeling observed in animal models such as guanylyl cyclase-A knockout (GC-A KO) mice,[4] β_1-adrenergic receptor–overexpressing transgenic (Tg) mice,[5] and spontaneously hypertensive rats.[6] However, many signal transduction pathways are activated in these models; therefore, whether activation of NHE1 alone is sufficient to induce hypertrophy remains unknown. We also lack detailed understanding of the molecular and cellular events, including altered intracellular Na^+

Original received March 5, 2008; revision received August 21, 2008; accepted August 25, 2008.

From the Departments of Molecular Physiology (T.Y.N., Y.I., S.W.), Bioscience (Y.A.), and Cardiovascular Dynamics (K.K.), National Cardiovascular Center Research Institute, Osaka, Japan.

*Both authors contributed equally to this work.

Correspondence to Shigeo Wakabayashi, Department of Molecular Physiology, National Cardiovascular Center Research Institute, Suita, Osaka 565-8565, Japan. E-mail wak@ri.ncvc.go.jp

Circulation Research is available at http://circres.ahajournals.org DOI: 10.1161/CIRCRESAHA.108.175141

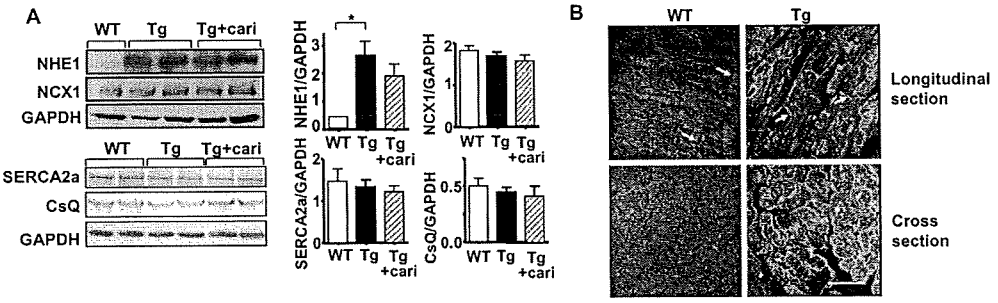

Figure 1. Overexpression of NHE1 protein in Tg hearts. A, Immunoblot analysis of NHE1 and other Ca^{2+} regulatory proteins normalized to endogenous GAPDH from WT, untreated, and cariporide-treated Tg hearts (n=7 hearts for each group). Two typical examples are shown in the each blot. B, Cellular localization of NHE1 proteins. Longitudinal and cross-sections of cardiac muscle from WT and Tg mice were immunostained with anti-NHE1 antibody. Arrows indicate the NHE1 localized to the intercalated disks. Scale bar=100 μm.

and/or Ca^{2+} handling and the activation of signaling pathways that result from NHE1 activation.

To directly address these questions, we generated Tg mice that overexpress an activated form of human NHE1 that lacks the calmodulin-binding inhibitory domain (Δ637 to 656)[7] under the control of cardiac α-myosin heavy chain promoter. Previously, we reported that deletion of this domain resulted in constitutive elevation of pH_i sensitivity in quiescent cells.[7,8] Here, we asked whether overexpressing this mutant form of NHE1 would affect development of cardiac hypertrophy and/or HF in vivo and investigated which signal transduction pathways were involved in NHE1-dependent cardiac pathogenesis. We present evidence that NHE1 serves as an important signal mediator in initiating cardiac remodeling and HF via activation of a Ca^{2+}-dependent hypertrophic pathway.

Materials and Methods

All animal experiments were carried out according to guidelines of the Animal Welfare Committee of the National Cardiovascular Center Research Institute. Tg mice that overexpressed an activated form of NHE1 (human NHE1 with amino acids 637 to 656 deleted) were generated from C57BL/6J mice according to standard procedures; the expression of the transgene was under control of the murine cardiac α-myosin heavy chain promoter. The pH_i, $[Na^+]_i$, and Ca^{2+} transients in isolated adult myocytes were measured in Hepes- or bicarbonate-buffered Tyrode solutions by epifluorescent analysis [acetoxymethyl forms of 2′,7′-bis (carboxy-ethyl)-5- (and -6)-carboxyfluorescein (BCECF), sodium-binding benzofuran isophtalate (SBFI), and Indo-1, respectively] using an imaging system (AQUACOSMOS, Hamamatsu Photonics). Data are presented as means±SD or SEM of at least 3 determinations. We used the paired or unpaired *t* test for statistical analyses. Values of $P<0.05$ were considered statistically significant (indicated as * versus wild-type [WT] or † versus no-cariporide control, or as otherwise indicated). An expanded Materials and Methods section is available in the online data supplement at http://circres.ahajournals.org.

Results

Overexpression of Activated NHE1 Induces Cardiac Hypertrophy and HF In Vivo

We confirmed a marked increase (≈5-fold) in NHE1 protein levels in Tg hearts by immunoblot analysis (Figure 1A). Immunofluorescence analysis of tissue sections revealed that whereas WT hearts expressed low but detectable levels of NHE1 localized to intercalated discs, Tg hearts expressed much higher levels of NHE1 in both intercalated discs and sarcolemma (Figure 1B).

Overexpression of NHE1 in vivo resulted in cardiac hypertrophy and dilated cardiomyopathy; the Tg mouse hearts had thinner ventricular walls and greater chamber

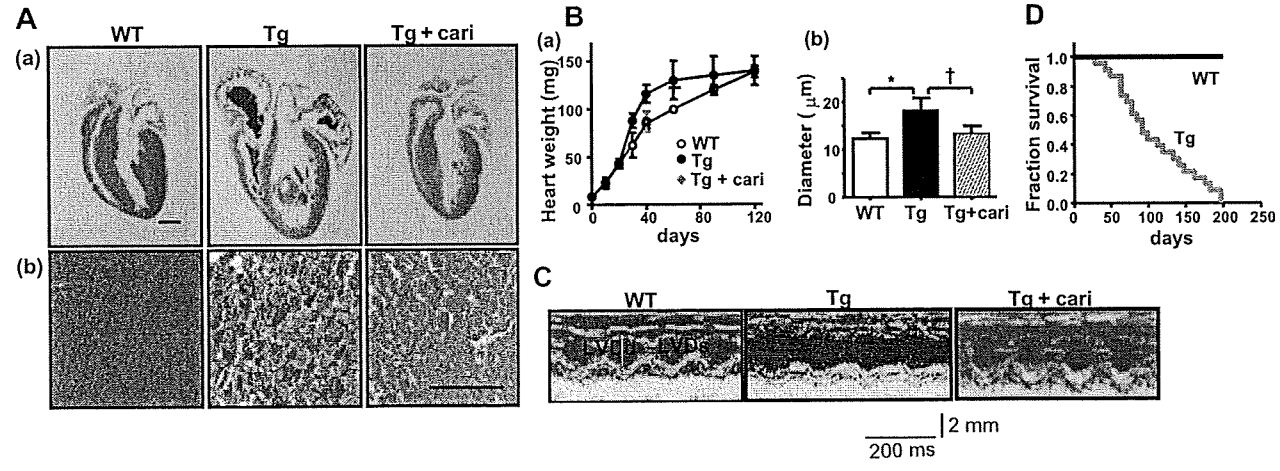

Figure 2. Overexpression of activated NHE1 results in cariporide-preventable cardiac hypertrophy, fibrosis, and HF. A, Cardiac sections stained with Masson trichrome. Scale bars: 1 mm (a) and 100 μm (b). B, Quantitative analysis of heart weight during development (a) and cardiomyocyte diameters (b) in WT, untreated, and cariporide-treated Tg hearts (n=5 separate hearts). C, Representative echocardiography obtained from each group. LVDd and LVDs indicate left ventricular dimension at diastole and systole, respectively. D, Kaplan–Meier survival analysis of WT and Tg mice. All results were obtained from 40-day-old mice, except in B (a) and D.

Table. Histological and Echocardiographic Analyses of Left Ventricular Dimensions and Function

	WT	Tg	Tg+Cariporide
Histopathology			
IVSW, mm	1.21±0.03	0.75±0.12*	1.29±0.36†
LVFW, mm	1.18±0.03	0.83±0.08*	1.35±0.32†
LV area, mm^2	1.95±0.30	6.07±0.84*	3.18±0.62†
Echocardiography			
LVDd, mm	2.44±0.15	3.27±0.46*	2.30±0.32†
LVDs, mm	0.56±0.02	1.98±0.04*	0.82±0.02†
% FS	77.8±8.0	33.0±5.3*	64.4±7.2†

IVSW indicates interventricular septal wall; LVFW, left ventricular free wall; LV area, LV surface area measured in short axis at widest section; LVDd, LV dimension at diastole; LVDs, LV dimension at systole; FS, fractional shortening. Values are means±SD; n=5–8 separate hearts for each group. *P<0.05 vs WT; †P<0.05 vs untreated Tg mice.

dilation accompanied by ventricular fibrosis (Figure 2A, supplemental Figure IB and the Table). We detected the onset of progressive hypertrophy in Tg hearts beginning at the age of 20 days (Figure 2B, a), with outstanding enlargement of the atria (supplemental Figure I A). Cardiomyocyte diameters in Tg mice were significantly larger than those in WT mice (Figure 2B, b). These results suggest that each myocyte became bigger at approximately 40 days of age, but they progressively died, as evidenced by chamber dilation. Echocardiography of Tg mice at 40 days of age showed increased diastolic and systolic ventricular diameters and decreased systolic function, which was demonstrated by a decrease in the percentage of fractional shortening (Figure 2C and the Table). Markers of HF, atrial natriuretic peptide, and cardiac troponin I in serum were also increased in Tg mice (supplemental Figure IC and ID), indicating that their hearts had developed HF. Tg mice had a high mortality rate (Figure 2D) and showed cardiac arrhythmia; this was particularly so for older mice (data not shown). However, all cardiac remodeling events observed in Tg mice were largely prevented by IP administration of cariporide for 20 days (from the age of 20 to 40 days; Figure 2, supplemental Figure I, and the Table) without significant change in NHE1 protein levels (Figure 1A), suggesting that these phenomena resulted from elevated NHE1 activity.

Overexpression of NHE1 did not significantly change the expression levels of other Ca^{2+} regulatory proteins (NCX1, sarcoplasmic reticulum Ca^{2+}-pump [SERCA2a], or calsequestrin [CsQ]) with or without cariporide treatment (Figure 1A). In addition, expression of Na^+/K^+-ATPase was also unchanged (WT, 0.36±0.04; Tg, 0.35±0.05; and Tg+cariporide, 0.40±0.07; n=3 hearts). As predicted from our previous work,[9] we detected a marked increase in the expression of calcineurin homologous protein (CHP)1, an obligatory subunit of NHE family members (supplemental Figure IIA),[10] concomitant with the high level of NHE1 expression in Tg mice.

Increased Exchange Activity and $[Na^+]_i$ in Cardiomyocytes from Tg Mice

We measured pH_i and $[Na^+]_i$ in freshly isolated ventricular myocytes from WT and Tg hearts. Tg myocytes appeared to be more vulnerable to collagenase treatment and mechanical stress than WT myocytes. Surviving Tg myocytes were larger than WT myocytes (Figure 3A), similar to our observations in whole-heart sections (Figure 2B). In addition, the pH_i recovery of Tg myocytes after acid loading that was cariporide-inhibitable was faster than that of WT myocytes (Figure 3B). Consistent with our previous data using this NHE1 mutant,[7,8] the pH_i dependence of the H^+ efflux rate (J_H) was alkaline-shifted in Tg myocytes (Figure 3C) after correction for the intracellular H^+ buffering power, which was similar between

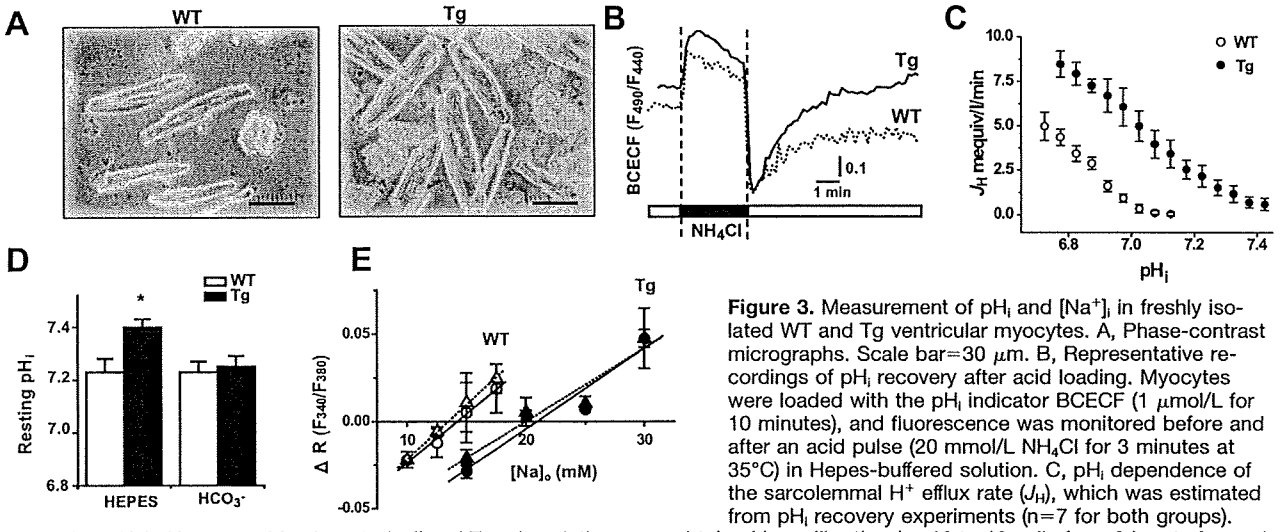

Figure 3. Measurement of pH_i and $[Na^+]_i$ in freshly isolated WT and Tg ventricular myocytes. A, Phase-contrast micrographs. Scale bar=30 μm. B, Representative recordings of pH_i recovery after acid loading. Myocytes were loaded with the pH_i indicator BCECF (1 μmol/L for 10 minutes), and fluorescence was monitored before and after an acid pulse (20 mmol/L NH_4Cl for 3 minutes at 35°C) in Hepes-buffered solution. C, pH_i dependence of the sarcolemmal H^+ efflux rate (J_H), which was estimated from pH_i recovery experiments (n=7 for both groups). D, Resting pH_i in Hepes- or bicarbonate-buffered Tyrode solutions was obtained by calibration (n=16 to 19 cells from 6 hearts for each group [see also supplemental Figure IV]). E, Evaluation of resting $[Na^+]_i$ in Hepes-buffered (dotted lines) or bicarbonate-buffered (solid lines) solution in WT (open symbols) and Tg myocytes (closed symbols), using the Na^+-specific fluorophore SBFI and the null-point approach. Average changes in SBFI ratio (ΔR) vs $[Na^+]_o$ were fitted, and linear regressions for all points provided the resting $[Na^+]_i$ (n=25 and 12 cells for each point from 4 Tg and 4 WT hearts, respectively).

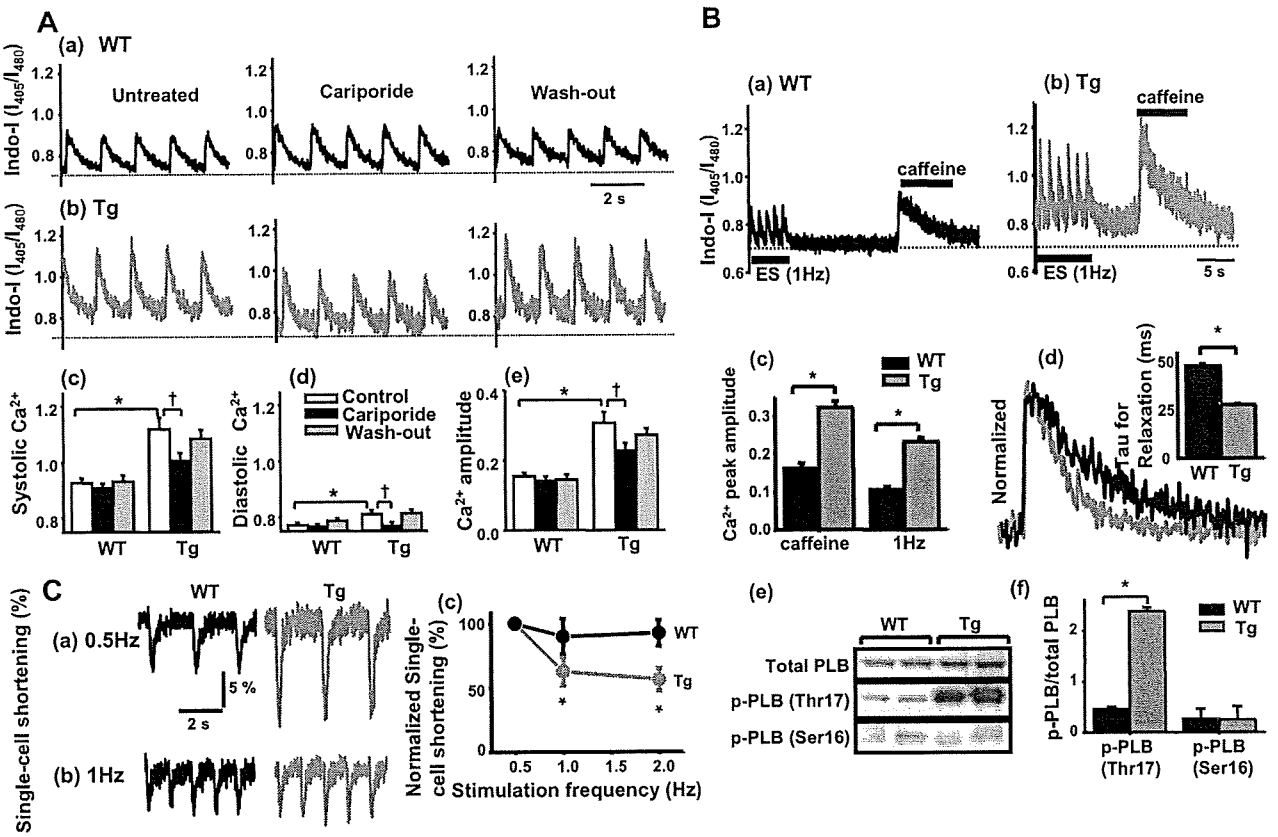

Figure 4. Comparison of the intracellular Ca^{2+} levels, SR Ca^{2+} content, and the amount of single-cell shorting between WT and Tg myocytes. A, Intracellular Ca^{2+} transient and acute effects of cariporide. Representative traces of the Indo-1 ratio in single cardiomyocytes stimulated at 1 Hz from WT (a) and Tg mice (b) under baseline conditions (left), 2 minutes after cariporide (1 μmol/L) treatment (middle), and 2 minutes after drug washout (right). c through e, Average data representing the systolic (c), diastolic (d), and peak amplitude (e) of Ca^{2+} transients for each condition (n=26 and 18 cells from 3 WT and 3 Tg hearts, respectively). B, a through c, Estimation of SR Ca^{2+} content. Indo-1–loaded, paced (1 Hz) cardiomyocytes were briefly exposed to 10 mmol/L caffeine to monitor SR Ca^{2+} release. Representative traces for WT myocytes (a), Tg myocytes (b), and the averaged data (c) (n=10 and 14 cells from 3 WT and 3 Tg hearts, respectively). d, Faster Ca^{2+} decline in Tg myocytes. Ca^{2+} transients (0.5 Hz) were normalized and the time constants (tau) were obtained by fitting the decline phase with the first-order exponential decay (inset) (n=21 and 52 transients from 3 WT and 3 Tg hearts, respectively). e and f, PLB in Tg hearts was highly phosphorylated by CaMKII but not by PKA. Representative immunoblots of total and phosphorylated PLBs (e) and normalized phosphorylated levels (f) (n=4 independent blots from 2 WT and 2 Tg hearts for all conditions). C, Percentage of single-cell shortening elicited by different stimulation frequencies, 0.5 Hz (a) and 1 Hz (b). c, Each measurement made at a different stimulation frequency was normalized to the maximal value and then averaged (n=7).

WT and Tg myocytes (supplemental Figure III). In addition, the resting pH_i was significantly higher in Tg myocytes under bicarbonate-free conditions (pH_i 7.40 versus pH 7.23 in WT; Figure 3D), indicating that overexpressing the active NHE1 mutant led to elevated NHE activity. However, under bicarbonate-buffered conditions, the pH_i was not significantly different between WT and Tg myocytes (Figure 3D, see also supplemental Figure IV), suggesting that pH_i was compensated by bicarbonate-dependent mechanisms. According to the pH dependence of J_H, we can assume that the steady-state exchange activity would be higher in Tg than WT myocytes at the given resting pH_i under physiologically relevant bicarbonate conditions. Indeed, fluorescence measurements using the null-point method[11] revealed that $[Na^+]_i$ was almost 1.5-fold higher in Tg myocytes (17 to 21 mmol/L) than in WT myocytes (12 to 13 mmol/L) under both bicarbonate- and Hepes-buffered conditions (Figure 3E). Treatment with cariporide resulted in a rapid reduction of $[Na^+]_i$ in Tg myocytes, which reached the value close to the WT myocytes (supplemental Figure V). Thus, elevation in $[Na^+]_i$ rather than pH_i would be the important event caused by NHE1 activation under physiological conditions.

Tg Myocytes Exhibited Increased Ca^{2+} Levels in the Cytoplasm and Sarcoplasmic Reticulum

As shown in Figure 4A, at 1-Hz stimulation, both diastolic and systolic Ca^{2+} levels were significantly higher in Tg than in WT cardiomyocytes (179±22.7 and 486±18.4 nmol/L in WT and 263±15.8 and 1142±41 nmol/L in Tg myocytes, respectively); Ca^{2+} amplitude (difference between the diastolic and systolic Ca^{2+} levels) was also 2-fold higher in Tg myocytes. Treatment with 1 μmol/L cariporide for 2 minutes, which led to 70% to 80% inhibition of NHE1 activity (data not shown), had little effect on Ca^{2+} transients in WT cardiomyocytes, whereas all parameters (diastolic, systolic, and Ca^{2+} amplitude) were at least partly decreased in Tg cardiomyocytes. Two-minute washout reversed the effects of cariporide, suggesting that the increase in intracellular Ca^{2+}

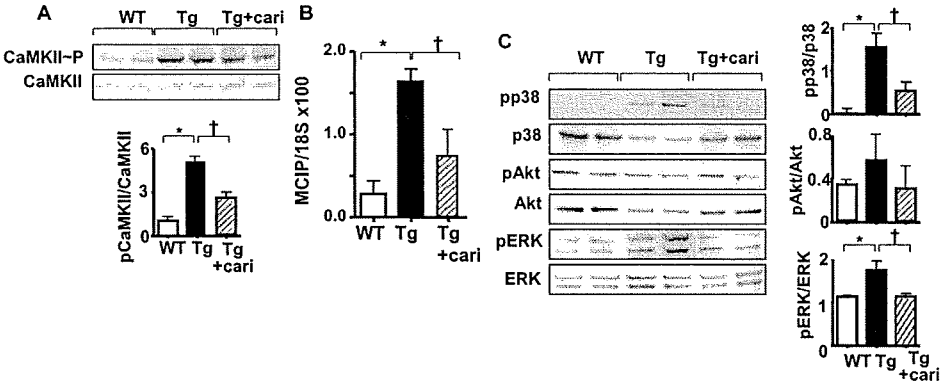

Figure 5. Activation of CaMKII, calcineurin, and p38 signaling pathways related to cardiac hypertrophy in Tg mice. A and C, Relative amounts of phosphorylated CaMKII, p38, Akt, and ERK42/44 were normalized to total protein. B, mRNA level of modulatory calcineurin inhibitory protein-1 (MCIP1), which was used as an indicator of activated calcineurin, was quantified by quantitative RT-PCR (n=7 hearts).

levels in Tg myocytes was attributable to increased NHE1 activity. Furthermore, we also detected marked elevations in diastolic and systolic Ca^{2+} levels at more physiologically relevant stimulation frequencies (up to 3.3 Hz), especially in Tg myocytes; Ca^{2+} amplitude was also significantly higher in Tg myocytes at all stimulation frequencies tested (supplemental Figure VI).

Furthermore, the peak amplitude of the caffeine-induced Ca^{2+} transient, which we used as an index of sarcoplasmic reticulum (SR) Ca^{2+} content, was ≈2-fold higher in Tg versus WT myocytes (Figure 4B, a through c), suggesting that this is one of the mechanisms of increased $[Ca^{2+}]_i$ in Tg myocytes. The rate of decline in the field stimulation-elicited Ca^{2+} transient was significantly faster in Tg than in WT myocytes (Figure 4B, d): the time constant (tau) was reduced to ≈60% (inset), indicating accelerated Ca^{2+} removal, mainly by SR Ca^{2+} pumping. In addition, the Ca^{2+} transient upstroke was faster in Tg myocytes than in WT myocytes (supplemental Figure VII), suggesting that the rate of Ca^{2+} release from the SR may also be higher in Tg myocytes. Ca^{2+}/calmodulin-dependent protein kinase (CaMK)II-dependent Thr17 phosphorylation of phospholamban (PLB), a Ca^{2+} pump regulatory protein, was almost 5-fold greater in Tg hearts than in WT hearts, yet no difference was detected at Ser16, a protein kinase (PK)A phosphorylation site (Figure 4B, e and f), strongly suggesting that CaMKII, but not PKA, is activated in Tg hearts and induces PLB phosphorylation, leading to enhanced SR Ca^{2+} loading and subsequent increase in cytoplasmic Ca^{2+} levels.

Effects on Single-Cell Shortening

We measured single-cell shortening in the same myocyte from which the Ca^{2+} transient was obtained, stimulated over a range of frequencies (0.5–2.0 Hz). Interestingly, we observed a clear frequency-dependent decrease in contractility in Tg myocytes after normalizing to the maximal value, although the actual single-cell shortening (percentage) was greater in the Tg than in the WT group at low stimulation frequency (0.5 Hz; Figure 4C). In addition, we observed that Tg myocytes were more susceptible to high frequency stimulation-induced cytotoxicity (supplemental Figure VIIIA). These results indicate that contractile dysfunction occurs at the cellular level in Tg myocytes.

Activation of Prohypertrophic Molecules in Tg Mice

We assessed the activity of 2 Ca^{2+}-dependent prohypertrophic signaling molecules, CaMKII and calcineurin,[12] in Tg hearts. The level of phosphorylated CaMKII was markedly increased (Figure 5A), consistent with increased CaMKII-dependent phosphorylation of PLB (Figure 4B, e and f). In addition, the amounts of mRNA (Figure 5B) and protein (supplemental Figure IIB) of MCIP1 (modulatory calcineurin inhibitory protein-1), which was used as a sensitive indicator of calcineurin activity, was significantly elevated in Tg hearts. Cariporide largely prevented both effects, suggesting that both CaMKII and calcineurin activation were NHE1-dependent. Furthermore, we detected a marked increase in the phosphorylation of p38, as well as a slight but significant increase in the phosphorylated active forms of extracellular signal-regulated kinase (ERK)42/44 mitogen-activated protein kinases (MAPKs), which were both largely reversed by cariporide treatment. Akt also appeared to be slightly activated in Tg hearts, although this was not statistically significant (Figure 5C).

NHE1-Dependent Translocation of HDAC and NFAT

Calcineurin is known to induce nuclear translocation of the NFAT family of transcription factors during hypertrophy via its dephosphorylation,[13] whereas CaMKII has been reported to induce nuclear export of histone deacetylase (HDAC)4 by phosphorylating it and thereby promote cardiomyocyte hypertrophy by blocking HDAC-dependent inhibition of target gene transcription.[14] To determine whether these pathways were activated by NHE1 overexpression, we treated primary cultured neonatal rat ventricular myocytes (NRVMs), which are often used as a model system of pathological hypertrophy, with a hypertrophic stimulus from phenylephrine and found that it induced a clear translocation of HDAC4 from the nucleus to the cytoplasm in these cells (supplemental Figure IX). Strikingly, overexpression of NHE1 also triggered translocation of HDAC4–green fluorescent protein (HDAC4-GFP) from the nucleus to the cytoplasm (Figure 6A, a) to an extent similar to that detected in phenylephrine-treated myocytes (Figure 6A, c) and redistributed from the cytoplasm to the nucleus on treatment with cariporide (10 μmol/L for at least 3 hours; Figure 6A shows the same myocyte before and

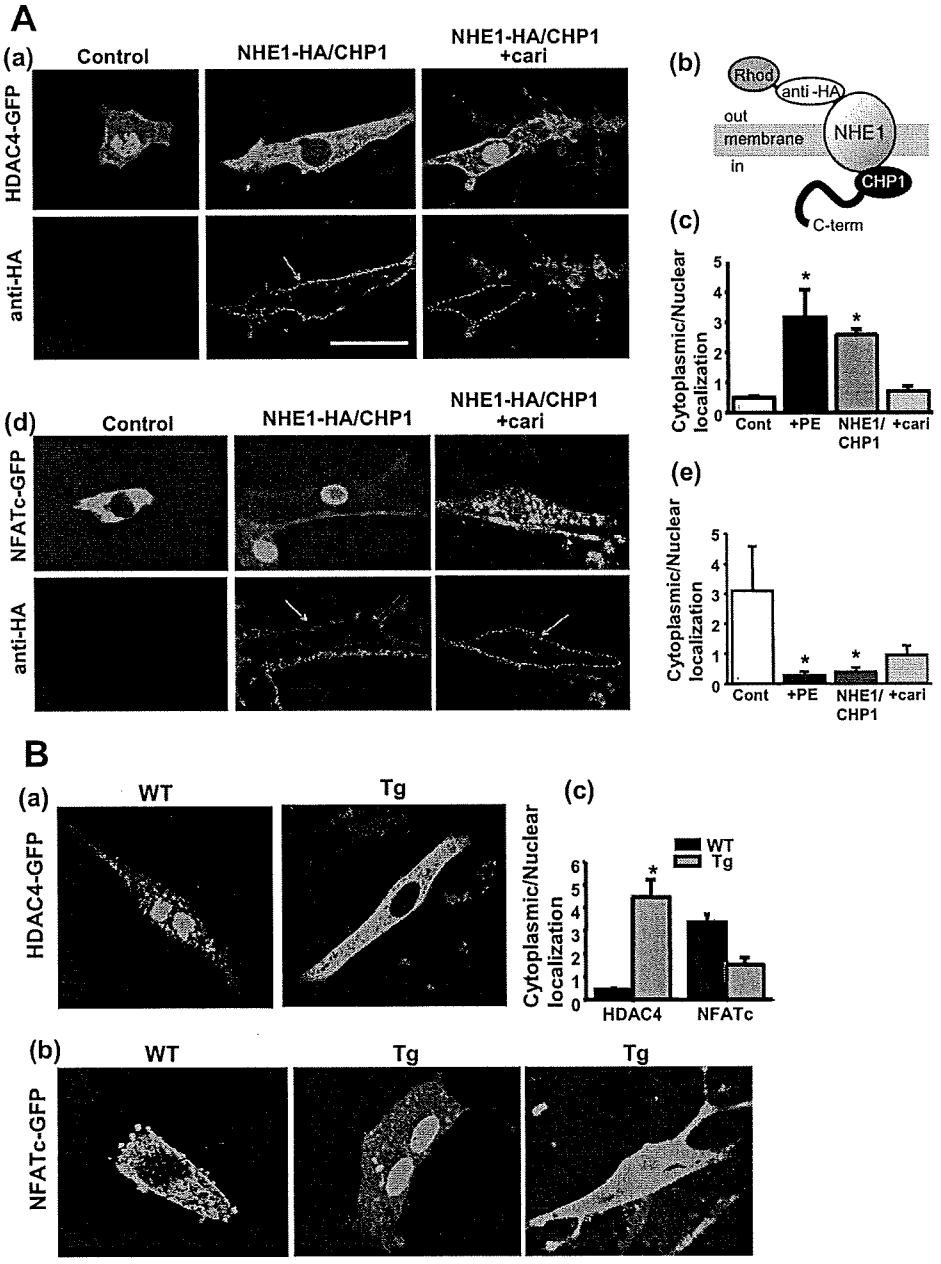

Figure 6. NHE1-dependent subcellular localization of HDAC4 and NFAT. A, a through c, Primary cultured NRVMs were cotransfected with HDAC4-GFP and NHE1-HA (tagged extracellularly) plus its obligatory subunit CHP1 (NHE1-HA/CHP1) or an empty vector. Two days later, NHE1-overexpressing living myocytes were visualized by indirect immunofluorescence (red), and the subcellular localization of HDAC4-GFP was quantified by confocal microscopy (green). Positions of some NHE1-overexpressing cells were marked, and then the same myocyte was chased after cariporide application (10 μmol/L, ≈3 hours). d and e, Similar experiments were performed for NFAT-GFP (*P<0.05 vs control). B, Tg myocytes exhibit full activation of the CaMKII-HDAC pathway but only partial activation of the calcineurin–NFAT pathway. Neonatal WT and Tg myocytes cultured for 2 days were transfected with HDAC4-GFP or NFAT-GFP. The subcellular localization of GFP in cardiomyocytes was examined 2 days later (n≥20 cells from 3 independent preparations). Scale bar=20 μm.

after cariporide treatment). Similar NHE1-dependent cytoplasmic accumulation of HDAC4 was observed for endogenous HDAC4 (supplemental Figure IXB). These results strongly suggest that overexpression of NHE1 promotes CaMKII-HDAC signaling. Furthermore, overexpression of NHE1 resulted in nuclear import of NFAT-GFP from the cytoplasm, as observed in the phenylephrine-treated group; this was partially reversed by cariporide treatment (Figure 6A, d and e). These results suggest that overexpression of NHE1 activated the calcineurin–NFAT pathway.

We performed similar experiments in primary cultured mouse ventricular myocytes from WT and Tg hearts. As shown in Figure 6B, HDAC4-GFP accumulated in the cytoplasm of Tg myocytes, whereas it was localized to the nucleus in WT myocytes, as was the case for the NHE1-overexpressing NRVMs (see also supplemental Figure IXC). On the other hand, NFAT-GFP localized to the cytoplasm in WT cells, but in Tg myocytes, its localization was somewhat intermediate: some localized to the nucleus and some to the cytoplasm (Figure 6B, b and c, for averaged data). These results indicate that the CaMKII-HDAC pathway is fully activated but that the calcineurin–NFAT pathway is only partially activated in Tg myocytes, suggesting that a more complex regulatory mechanism exists in Tg hearts.

Discussion

Despite accumulating evidence of a pathological role for NHE1 in cardiac hypertrophy, remodeling, and HF, it was not known whether direct activation of NHE1 itself could induce

these states. Here, we demonstrated that NHE1 activation is sufficient to initiate these cardiac disease states via activation of Ca^{2+}-dependent prohypertrophic signaling pathways and possibly via acceleration of Ca^{2+}-induced cell death. This conclusion is supported by a number of novel findings from our mouse model: (1) overexpression of an activated form of NHE1 (Δ637 to 656) resulted in cardiac hypertrophy followed by dilated cardiomyopathy in vivo; (2) in isolated Tg myocytes, $[Na^+]_i$ was increased because of enhanced Na^+/H^+ exchange activity, and both diastolic and systolic Ca^{2+} levels were significantly elevated but with less contractility at higher stimulation frequencies; (3) such remodeling was accompanied by activation of Ca^{2+}-dependent prohypertrophic pathways CaMKII-HDAC and calcineurin–NFAT, as well as p38 and ERK42/44 MAPKs; and (4) these effects observed in vivo and in vitro were largely prevented by cariporide. Because NHE1 is activated by numerous extracellular stimuli, these findings support the view that NHE1 plays an important role in transducing extracellular stimuli into intracellular Ca^{2+} signals, and therefore has a great impact on cardiac pathogenesis.

Elevated $[Ca^{2+}]_i$ in Tg Myocytes: Mechanisms and Consequences

The increased resting pH_i and accelerated net H^+ efflux under Hepes-buffered conditions provided direct evidence for enhanced Na^+/H^+ exchange activity in Tg myocytes. Furthermore, we observed that $[Na^+]_i$ were elevated in Tg myocytes under both bicarbonate-buffered and bicarbonate-free conditions, although no significant changes in pH_i were detected between WT and Tg myocytes under bicarbonate buffer. These findings suggest that the increased $[Na^+]_i$ rather than pH_i would be an initial signal to trigger the phenotypic changes in myocytes, consistent with previous reports demonstrating the relative importance of increased $[Na^+]_i$ in cardiac hypertrophy and HF.[15–18] Although the expression level of NCX1 protein was unchanged in our Tg hearts, increased $[Na^+]_i$ would have influenced the driving force and hence the activity of the NCX by decreasing the forward (Ca^{2+} efflux) and/or increasing the reversed mode (Ca^{2+} influx), resulting in increased $[Ca^{2+}]_i$, as reported previously.[18] In fact, we observed that both systolic and diastolic Ca^{2+} levels were significantly increased in Tg myocytes and that these levels were further pronounced at higher stimulation frequencies. Previous reports showed that $[Na^+]_i$ in failing myocardium, which is significantly higher than that in nonfailing myocardium, increases more in response to a higher stimulation frequency in both rats and humans.[19,20] Rapid stimulation-induced membrane depolarization can further activate the reverse mode of NCX1 and promote diastolic Ca^{2+} overload.

Furthermore, we present evidence of altered SR Ca^{2+} handling in Tg hearts, which involved CaMKII-dependent phosphorylation of PLB and subsequent activation of SERCA2a, leading to a higher rate of SR Ca^{2+} pumping. In addition to the higher SR Ca^{2+} content, CaMKII-induced phosphorylation and activation of the ryanodine receptor[21] might also be involved in the accelerated Ca^{2+} release from the SR in Tg myocytes. Thus, overexpression of NHE1 results in both (1) increased diastolic Ca^{2+} levels and (2) altered SR Ca^{2+} handling. A continuous increase in diastolic Ca^{2+} could activate critical hypertrophic signaling mechanisms and could trigger some death signals. Although reduced SR Ca^{2+} handling is often reported in failing hearts,[22] in the case of NHE1 Tg myocytes, the combination of Na^+-induced diastolic Ca^{2+} overload and enhanced SR Ca^{2+} pumping would ultimately lead SR Ca^{2+} overload, which itself has been reported to activate some Ca^{2+}-dependent protease calpains and induce apoptosis through the mitochondrial death pathway involving BAD, Bid, and caspase12[23]; we observed marked degradation of cardiac troponin I in Tg heart (supplemental Figure IIC), which might be a consequence of such an event. Thus, it is plausible that both Na^+-induced diastolic Ca^{2+} overload and enhanced SR Ca^{2+} pumping promote HF in Tg hearts.

As has been observed in human failing hearts,[1] we observed negative force–frequency dependence in Tg myocytes (see Figure 4C) without any change in the diastolic cell length (data not shown). Preservation of the high Ca^{2+} amplitude relative to diminished contractility observed in Tg mice at high stimulation frequency within the same myocyte suggests that myofibril Ca^{2+} sensitivity might be decreased. Possible mechanisms of this phenomenon are presently unknown. However, a recent report demonstrated that a reduction in myofilament Ca^{2+} sensitivity was introduced by PKD-dependent cardiac troponin I phosphorylation,[24] which may occur in cardiac disease states.[25] We also detected a slight but significant increase in the phosphorylation of troponin I in Tg hearts (supplemental Figure VIIIB).

Overall, the results of the single-cell experiments suggest the cellular mechanisms of hypertrophy/HF observed in vivo. However, we must consider that in vivo hearts consist of a heterogeneous population of cardiomyocytes that includes dead cells that are not available for in vitro experiments after cell isolation.

Downstream Signaling Pathways Leading to Cardiac Hypertrophy and HF

Numerous signaling pathways are known to coordinate pathological hypertrophy and HF, including calcineurin and CaMKII, PKC, and MAPKs (ERK42/44, ERK5, p38, and JNK).[12] We found that the Ca^{2+}-dependent signaling molecules CaMKII and calcineurin are both highly activated in Tg hearts and that this activation was reversed by cariporide treatment. These findings suggest that NHE1, coupled with NCX1, can supply a Ca^{2+} source for activating both the CaMKII and calcineurin pathways. Indeed, recent reports have suggested that both NCX[18] and calcineurin[26] are involved in endothelin-1–induced hypertrophy in rat myocytes, secondary to NHE1 activation. Furthermore, overexpression of NHE1 triggered nuclear export of HDAC and nuclear import of NFAT in a cariporide-sensitive manner, providing direct evidence that alterations in the sarcolemmal Na^+/H^+ exchange activity can modulate hypertrophy-associated gene expression in cardiomyocytes.

In contrast to the exclusive NHE1-dependent translocation patterns of NFAT and HDAC in NRVMs, NFAT was incompletely nuclear translocated in Tg myocytes, suggesting

that activation of NFAT was partially blocked in Tg myocytes despite calcineurin activation. In addition to Ca^{2+}-dependent pathways, we found that p38 and ERK42/44 MAPKs were significantly activated in Tg hearts. Because p38 (as well as GSK3β, the downstream molecule of Akt) is known to negatively regulate calcineurin–NFAT signaling via phosphorylation of NFAT,[12] we assume that p38 activation would be one of the mechanisms for partial activation of the NFAT signal in Tg myocytes. This is consistent with the recent finding that CaMKII rather than calcineurin might serve as a major NHE1-dependent hypertrophy molecule in GC-A KO mice.[4] Indeed, overexpression of activated CaMKII itself results in pronounced hypertrophy and dilated cardiomyopathy.[27] Because p38 activation could have been caused by stress and/or receptor activation secondary to enhanced mechanical load, we do not exclude the possibility that the calcineurin pathway predominates in the initial period of hypertrophy, as previously reported.[26]

Pathological Implications of NHE1 in Cardiac Hypertrophy and HF

NHE1 activity is upregulated in several in vivo and in vitro models of cardiac hypertrophy/HF,[4,5,28] and NHE1 inhibitors prevent the detrimental effects,[2] suggesting that NHE1 contributes to cardiac remodeling. Consistent with these reports, we directly demonstrated that NHE1 activation is sufficient to induce hypertrophy and HF; however, there are also some differences between our model and those used in other studies. For example, hearts of GC-A KO mice exhibit hypertrophy but do not develop HF.[4] This may be a matter of the degree of NHE1 activation, because the expression level of NHE1 protein was unchanged in GC-A KO mice. In addition, there was a significant increase in p38 phosphorylation in our Tg hearts. Because it has been shown that p38 activation in MKK3 or MKK6 Tg mice induced dilated cardiomyopathy and HF without causing hypertrophy,[29] it is possible that there are independent mechanisms for inducing hypertrophy and HF, both of which might be activated in our mouse model (supplemental Figure X).

Our data suggest that NHE1-induced Na^+ overload and altered Ca^{2+} handling are sufficient to introduce cardiac hypertrophy mainly through activation of the CaMKII-HDAC4 pathway. Whether or not this is "the necessary event" remains to be determined. However, our results do demonstrate that NHE1 activation can be an initiation signal to promote cardiac remodeling.

Acknowledgments

We thank Dr Munekazu Shigekawa (Senri Kinran University) and Dr William Coetzee (New York University School of Medicine) for fruitful discussions about the manuscript. We also thank Hitomi Otake and Madoka Hirayama for technical assistance.

Sources of Funding

This work was supported by Grants-in-Aid for Priority Areas 18077015 and 18059053; grants-in-aid 19390080, 19590220, 18590796; a grant for the Cooperative Link for Unique Science and Technology for Economy Revitalization from the Ministry of Education, Culture, Sports, Science, and Technology of Japan; a grant for Promotion of Fundamental Studies in Health Sciences of the National Institute of Biomedical Innovation (NIBIO); research grants for Cardiovascular Diseases (17A-1) and for Nervous and Mental Disorders (16B-2 and 19B-1) from the Ministry of Health, Labor, and Welfare; Salt Science Research Foundation grant 0737; and a grant from the Takeda Science Foundation.

Disclosures

None.

References

1. Pieske B, Houser SR. $[Na^+]_i$ handling in the failing human heart. *Cardiovasc Res.* 2003;57:874–886.
2. Karmazyn M, Gan XT, Humphreys RA, Yoshida H, Kusumoto K. The myocardial Na^+-H^- exchange: structure, regulation, and its role in heart disease. *Circ Res.* 1999;85:777–786.
3. Avkiran M, Marber MS. Na^+-H^+ exchange inhibitors for cardioprotective therapy: progress, problems and prospects. *J Am Coll Cardiol.* 2002;39:747–753.
4. Kilic A, Velic A, De Windt LJ, Fabritz L, Voss M, Mitko D, Zwiener M, Baba HA, van Eickels M, Schlatter E, Kuhn M. Enhanced activity of the myocardial Na^+/H^+ exchanger NHE-1 contributes to cardiac remodeling in atrial natriuretic peptide receptor-deficient mice. *Circulation.* 2005;112:2307–2317.
5. Engelhardt S, Hein L, Keller U, Klambt K, Lohse MJ. Inhibition of Na^+-H^+ exchange prevents hypertrophy, fibrosis, and heart failure in $beta_1$-adrenergic receptor transgenic mice. *Circ Res.* 2002;90:814–819.
6. Perez NG, Alvarez BV, Camilion de Hurtado MC, Cingolani HE. pH_i regulation in myocardium of the spontaneously hypertensive rat. Compensated enhanced activity of the Na^+/H^+ exchanger. *Circ Res.* 1995;77:1192–1200.
7. Wakabayashi S, Bertrand B, Ikeda T, Pouyssegur J, Shigekawa M. Mutation of calmodulin-binding site renders the Na^+/H^+ exchanger (NHE1) highly H^+-sensitive and Ca^{2+} regulation-defective. *J Biol Chem.* 1994;269:13710–13715.
8. Wakabayashi S, Ikeda T, Iwamoto T, Pouyssegur J, Shigekawa M. Calmodulin-binding autoinhibitory domain controls "pH-sensing" in the Na^+/H^+ exchanger NHE1 through sequence-specific interaction. *Biochemistry.* 1997;36:12854–12861.
9. Pang T, Hisamitsu T, Mori H, Shigekawa M, Wakabayashi S. Role of calcineurin B homologous protein in pH regulation by the Na^+/H^+ exchanger 1: tightly bound Ca2+ ions as important structural elements. *Biochemistry.* 2004;43:3628–3636.
10. Pang T, Su X, Wakabayashi S, Shigekawa M. Calcineurin homologous protein as an essential cofactor for Na^+/H^+ exchangers. *J Biol Chem.* 2001;276:17367–17372.
11. Despa S, Islam MA, Pogwizd SM, Bers DM. Intracellular $[Na^+]$ and Na^+ pump rate in rat and rabbit ventricular myocytes. *J Physiol.* 2002;539:133–143.
12. Heineke J, Molkentin JD. Regulation of cardiac hypertrophy by intracellular signalling pathways. *Nat Rev Mol Cell Biol.* 2006;7:589–600.
13. Crabtree GR, Olson EN. NFAT signaling: choreographing the social lives of cells. *Cell.* 2002;109(suppl):S67–S79.
14. Backs J, Song K, Bezprozvannaya S, Chang S, Olson EN. CaM kinase II selectively signals to histone deacetylase 4 during cardiomyocyte hypertrophy. *J Clin Invest.* 2006;116:1853–1864.
15. Perez NG, de Hurtado MC, Cingolani HE. Reverse mode of the Na^+-Ca^{2+} exchange after myocardial stretch: underlying mechanism of the slow force response. *Circ Res.* 2001;88:376–382.
16. Schafer M, Schafer C, Michael Piper H, Schluter KD. Hypertrophic responsiveness of cardiomyocytes to alpha- or beta-adrenoceptor stimulation requires sodium-proton-exchanger-1 (NHE-1) activation but not cellular alkalization. *Eur J Heart Fail.* 2002;4:249–254.
17. Baartscheer A. Chronic inhibition of Na^+/H^+-exchanger in the heart. *Curr Vasc Pharmacol.* 2006;4:23–29.
18. Dulce RA, Hurtado C, Ennis IL, Garciarena CD, Alvarez MC, Caldiz C, Pierce GN, Portiansky EL, Chiappe de Cingolani GE, Camilion de Hurtado MC. Endothelin-1 induced hypertrophic effect in neonatal rat cardiomyocytes: involvement of Na^+/H^+ and Na^+/Ca^{2+} exchangers. *J Mol Cell Cardiol.* 2006;41:807–815.
19. Maier LS, Pieske B, Allen DG. Influence of stimulation frequency on $[Na^+]_i$ and contractile function in Langendorff-perfused rat heart. *Am J Physiol.* 1997;273:H1246–H1254.

20. Pieske B, Maier LS, Piacentino V III, Weisser J, Hasenfuss G, Houser S. Rate dependence of $[Na^+]_i$ and contractility in nonfailing and failing human myocardium. *Circulation.* 2002;106:447–453.
21. Ai X, Curran JW, Shannon TR, Bers DM, Pogwizd SM. Ca^{2+}/calmodulin-dependent protein kinase modulates cardiac ryanodine receptor phosphorylation and sarcoplasmic reticulum Ca^{2+} leak in heart failure. *Circ Res.* 2005;97:1314–1322.
22. Bers DM, Despa S, Bossuyt J. Regulation of Ca^{2+} and Na^+ in normal and failing cardiac myocytes. *Ann N Y Acad Sci.* 2006;1080:165–177.
23. Chen X, Zhang X, Kubo H, Harris DM, Mills GD, Moyer J, Berretta R, Potts ST, Marsh JD, Houser SR. Ca^{2+} influx-induced sarcoplasmic reticulum Ca^{2+} overload causes mitochondrial-dependent apoptosis in ventricular myocytes. *Circ Res.* 2005;97:1009–1017.
24. Cuello F, Bardswell SC, Haworth RS, Yin X, Lutz S, Wieland T, Mayr M, Kentish JC, Avkiran M. Protein kinase D selectively targets cardiac troponin I and regulates myofilament Ca^{2+} sensitivity in ventricular myocytes. *Circ Res.* 2007;100:864–873.
25. Harrison BC, Kim MS, van Rooij E, Plato CF, Papst PJ, Vega RB, McAnally JA, Richardson JA, Bassel-Duby R, Olson EN, McKinsey TA. Regulation of cardiac stress signaling by protein kinase D1. *Mol Cell Biol.* 2006;26:3875–3888.
26. Ennis IL, Garciarena CD, Escudero EM, Perez NG, Dulce RA, Camilion de Hurtado MC, Cingolani HE. Normalization of the calcineurin pathway underlies the regression of hypertensive hypertrophy induced by Na^+/H^+ exchanger-1 (NHE-1) inhibition. *Can J Physiol Pharmacol.* 2007;85:301–310.
27. Zhang T, Maier LS, Dalton ND, Miyamoto S, Ross J Jr, Bers DM, Brown JH. The deltaC isoform of CaMKII is activated in cardiac hypertrophy and induces dilated cardiomyopathy and heart failure. *Circ Res.* 2003;92:912–919.
28. Yokoyama H, Gunasegaram S, Harding SE, Avkiran M. Sarcolemmal Na^+/H^+ exchanger activity and expression in human ventricular myocardium. *J Am Coll Cardiol.* 2000;36:534–540.
29. Liao P, Georgakopoulos D, Kovacs A, Zheng M, Lerner D, Pu H, Saffitz J, Chien K, Xiao RP, Kass DA, Wang Y. The in vivo role of p38 MAP kinases in cardiac remodeling and restrictive cardiomyopathy. *Proc Natl Acad Sci U S A.* 2001;98:12283–12288.

ARTICLE IN PRESS

Biochemical and Biophysical Research Communications xxx (2008) xxx–xxx

Contents lists available at ScienceDirect

Biochemical and Biophysical Research Communications

journal homepage: www.elsevier.com/locate/ybbrc

Down-regulation of P-glycoprotein expression by sustained intracellular acidification in K562/DOX cells

Ying Lu [a], Tianxiang Pang [a,*], Jianxiang Wang [a], Dongsheng Xiong [a], Li Ma [a], Bin Li [a], Qinghua Li [a], Shigeo Wakabayashi [b]

[a] State key Laboratory of Experimental Hematology, Institute of Hematology and Hospital of Blood Diseases, Chinese Academy of Medical Sciences and Peking Union Medical College, Nanjing Road No. 288, Tianjin 300020, China
[b] Department of Molecular Physiology, National Cardiovascular Center Research Institute, Suita, Osaka 565-8565, Japan

ARTICLE INFO

Article history:
Received 24 September 2008
Available online xxxx

Keywords:
Multidrug resistance
P-glycoprotein
Na^+/H^+ exchanger1
Intracellular pH

ABSTRACT

We have investigated the involvement of intracellular pH (pH_i) in the regulation of P-glycoprotein (P-gp) in K562/DOX cells. The selective Na^+/H^+ exchanger1 (NHE1) inhibitor cariporide and the "high K^+" buffer were used to induce the sustained intracellular acidification of the K562/DOX cells that exhibited more alkaline pH_i than the K562 cells. The acidification resulted in the decreased P-gp activity with increased Rhodamine 123 (Rh123) accumulation in K562/DOX cells, which could be blocked by the P-gp inhibitor verapamil. Moreover, the acidification decreased MDR1 mRNA and P-gp expression, and promoted the accumulation and distribution of doxorubicin into the cell nucleus. Interestingly, these processes were all pH_i and time-dependent. Furthermore, the change of the P-gp expression was reversible with the pH_i recovery. These data indicate that the tumor multidrug resistance (MDR) mediated by P-gp could be reversed by sustained intracellular acidification through down-regulating the P-gp expression and activity, and there is a regulative link between the pH_i and P-gp in K562/DOX cells.

As the major obstacle of chemotherapy, MDR is mediated by P-gp, a 170 kDa membrane protein encoded by MDR1 gene, which leads to the chemoresistance and the decreased survival in leukemia's [1]. With the development of P-gp modulators to the third generation, the regulation of P-gp is still unsatisfactory [2]. Despite more than 30 years of research, the mechanisms underlying MDR reversal have not been fully clarified. Consequently, doing the future investigations of tumor MDR on a rational basis, and developing new strategies to overcome MDR upon this basis are especially necessary.

In recent years, it has been reported that cancer cells show a strong tendency towards an alkaline deviation of the entire homeostasis when they are resistant to therapeutic intervention [3–5], and malignant cells can live and multiply at pH_i levels from 7.46 to 7.6 and even higher [4,6]. This anomalous "malignant alkalosis" has already been considered to represent one of the most specific characters of the cancerous state by Reshkin and others [6,7]. Furthermore, a large variety of MDR modifiers known to be able to reverse resistance to chemotherapeutic drugs have been shown to exert their cellular effects through a pH-acidifying process; also, a decrease in pH_i has been shown to sensitize cancer cells of diverse origins to apoptosis and hyperthermia [8]. In all these cited cases, a cellular acid-base change is considered to be essential to break through drug resistance.

In order to clarify the internal correlation between pH_i and P-gp in MDR leukemia cells, we experimentally induced sustained intracellular acidification in K562 and K562/DOX cell lines with selective NHE1 inhibitor cariporide and the "high K^+" buffer method. Cariporide, a powerful and specific inhibitor of NHE1, could inhibit NHE1 and block the efflux of H^+ to achieve intracellular acidification [9]. The "high K^+" buffer method is widely used to induce intracellular acidification directly. It is suitable to acidify the cytoplasm for certain duration with little toxicity, and could also regulate the pH_i to the requested value [10,11].

We tested a potential role for sustained intracellular acidification in reversing of MDR through P-gp regulation, and assessed the possibility of a regulative link between pH_i and P-gp expression and activity. Our findings are the first results showing the reverse effect of MDR by sustained intracellular acidification in K562/DOX cells though P-gp regulation, and points out a regulative link between pH_i and P-gp expression. These findings suggest a novel role for pH_i in the regulation of MDR and provide important data for the further tumor MDR research.

Abbreviations: MDR, multidrug resistance P-gp, P-glycoprotein NHE1, Na^+/H^+ exchanger1 pH_i, intracellular pH Rh123, rhodamine 123 BCECF-AM, 2′, 7′-bis (2-carboxyethyl)-5 (6) -carboxyfluorescein acetoxymethyl

* Corresponding author. Fax: +86 22 23909093.
E-mail address: pang@ihcams.ac.cn (T. Pang).

0006-291X/$ - see front matter © 2008 Elsevier Inc. All rights reserved.
doi:10.1016/j.bbrc.2008.10.005

Please cite this article in press as: Y. Lu et al., Down-regulation of P-glycoprotein expression by sustained intracellular ..., Biochem. Biophys. Res. Commun. (2008), doi:10.1016/j.bbrc.2008.10.005

Materials and methods

Materials

RPMI 1640 media were purchased from Gibco-BRL Life Technologies, Inc. (Burlington, ON, Canada). Fetal bovine serum (FBS) was obtained from HyClone (Logan, UT). Human monoclonal antibody against P-gp, rabbit polyclonal antibody against GAPDH and horseradish peroxidase-conjugated anti-rabbit antibodies were obtained from Santa Cruz Biotechnology (Santa Cruz, CA). Enhanced Chemiluminescence Reagent Plus (ECL) reagents were from Santa Cruz Biotechnology (Santa Cruz, CA). Rhodamine 123 (Rh123), 2′,7′-bis(2-carboxyethyl)-5(6)-carboxyfluorescein acetoxymethyl (BCECF-AM), verapamil, doxorubicin and cariporide were purchased from Sigma (Shanghai, China).

Cell culture and experimental conditions

The MDR cell line K562/DOX was derived from K562 cells by selection in increased concentrations of doxorubicin. The derivative cell line was shown to have MDR phenotype by its elevated expression of P-gp, wide cross-resistance and defect in intracellular drug accumulation. K562 cells were cultured in RPMI 1640 with 10% (v/v) FBS, penicillin (50 U/ml), streptomycin (50 μg/ml) and L-glutamine (2 mmol/l) at 37 °C in humidified air with 5% CO_2. Medium for K562/DOX cells were further supplemented with doxorubicin 2 μmol/l. Prior to use in experiments, K562/DOX cells were cultured in drug-free medium for two weeks.

Measurement of pH_i and induction of intracellular acidification

Measurement of pH_i: pH_i of cells was assessed by flow cytometry using the pH-sensitive fluorescent probe BCECF-AM [12]. We did not observe any reduction of intracellular BCECF fluorescence intensities in K562 and K562/DOX cell lines, nor was loss of BCECF during the time course of the experiment in the two cell lines (data not shown). Cell suspensions in serum-free RPMI 1640 were washed and labeled with BCECF-AM. The labeled cells were analyzed with an excitation wavelength of 488 nm, and the ratio of the fluorescence at 530 and 640 nm was plotted vs. pH_i. In order to obtain the calibration curve, a linear regression within the pH_i range 6.2–7.4 was obtained.

Intracellular acidification: Cell suspensions in serum-free RPMI 1640 medium were washed and resuspended (1×10^6 cells/ml) with cariporide 3 mg/l in serum-free RPMI 1640 or the "high K^+" buffer containing H^+/K^+ ionophore nigericin 5 μmol/l to induce the pH_i to 7.2, 7.0 and 6.8 for 1 h and 3 h as described previously [10,11].

Real-time RT-PCR

Total RNAs were isolated from K562/DOX cells treated with cariporide 3 mg/l or "high K^+" buffer using TRIzol reagent (Invitrogen, San Diego, CA). Real-time PCR was done with 1 μl reverse transcription product in a MyiQ real-time PCR detection system (Bio-Rad, Hercules, CA) by using SYBR Green PCR Supermix (Bio-Rad). Human MDR1 primers were 5′-TGC TCA GAC AGG ATG TGA GTT G-3′ (forward) and 5′-TTA CAG CAA GCC TGG AAC CTA T-3′(reverse; 120 bp); Human GAPDH primers used as an internal control were

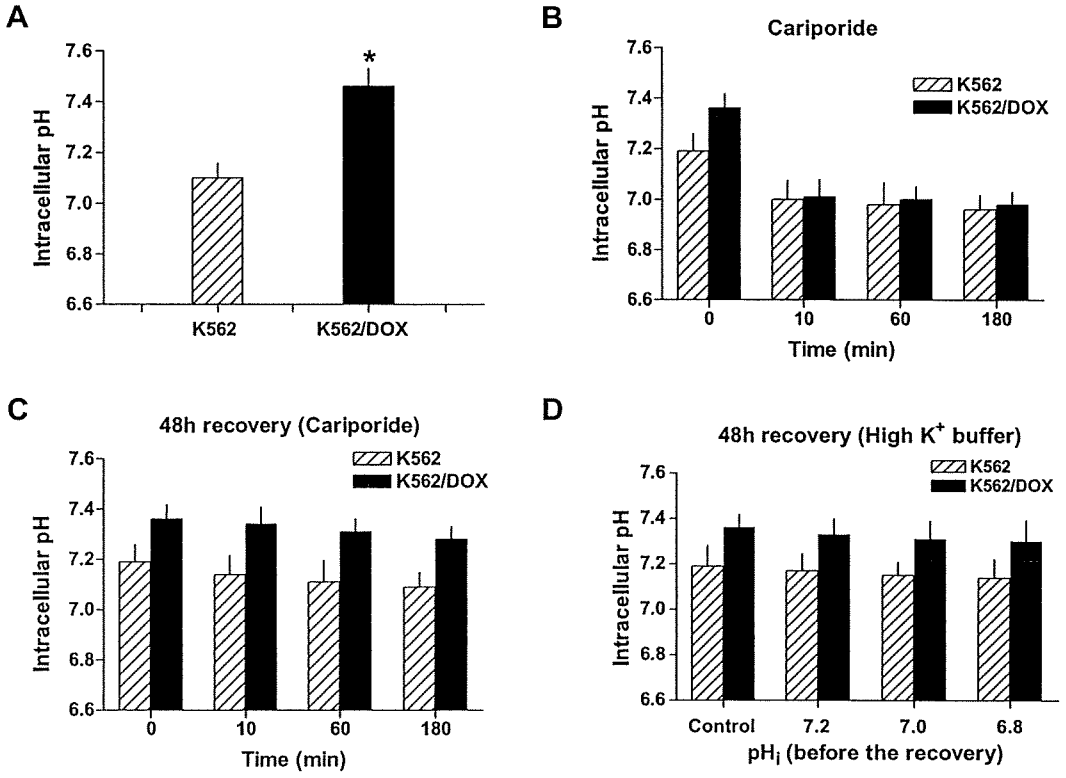

Fig. 1. Determination of pH_i in K562 and K562/DOX cells. (A) The pH_i of K562 and K562/DOX cells. (B) The pH_i of K562 and K562/DOX cells after treated with cariporide in 180 minutes. (C) The pH_i of K562 and K562/DOX cells after 48 h recovery from cariporide treatment for 3 h. (D) The pH_i of K562 and K562/DOX cells after 48 h recovery from "high K^+" buffer treatment for 3 h. Data represent means ± SD of results obtained from three different experiments performed in triplicate. Asterisks indicate statistical significance (p value <0.05, Student's t-test).

Please cite this article in press as: Y. Lu et al., Down-regulation of P-glycoprotein expression by sustained intracellular ..., Biochem. Biophys. Res. Commun. (2008), doi:10.1016/j.bbrc.2008.10.005

5′-GAA GGT GAA GGT CGG AGT-3′ (forward) and 5′-GAA GAT GGT GAT GGG ATT TC-3′ (reverse; 226 bp).

Western blotting

Proteins isolated from cell lines treated with cariporide 3 mg/l or the "high K^+" buffer were resolved by 6% SDS–PAGE and transferred onto polyvinylidene difluoride membranes (Millipore, Bedford, MA). The membranes were blocked for 1 h and then incubated first with primary antibodies and then horseradish peroxidase-conjugated secondary antibodies for 2 and 1 h, respectively. Specific proteins were visualized with enhanced chemiluminescence detection reagent and determined by densitometric analysis with a Lynx video densitometer (Biological Vision).

Flow cytometry and confocal laser microscopy

Flow cytometry was used to measure intracellular the fluorescent of P-gp substrate Rh123, which was transported by P-gp. After treated with cariporide 3 mg/l or the "high K^+" buffer for 3 hours, K562 and K562/DOX cells, with or without the pretreatment of verapamil 50 μmol/l for 30 min, were incubated for 1.5 h in serum-free RPMI 1640 containing Rh123 5 μmol/l. After incubation, the cells of each group were collected and resuspended in ice-cold PBS containing 1% fetal bovine serum and kept on ice until analysis by flow cytometry. In another group, K562 and K562/DOX cells treated with cariporide 3 mg/l or the "high K^+" buffer for 3 h were washed twice by Hepes buffer, and then treated with doxorubicin 10 μmol/l in serum-free RPMI 1640 for 1 h and washed twice by Hepes buffer before imaging on Bio-Rad 1024 confocal laser microscope.

Data analysis

Statistical analyses were made with Student's paired *t*-test using GraphPad Prism (San Diego, USA). Significance was assumed for *P* values less than 0.05.

Results

Intracellular pH of K562 and K562/DOX cells

The pH_i of K562/DOX cells was 7.46 while that of K562 cells was only 7.1 (Fig. 1A). After 3 h treatment with cariporide 3 mg/l, the pH_i of K562 and K562/DOX cells were both decreased to about 7.0 in 10 min, and the value changed little in the following 170 min. After 48 h recovery in normal culture condition, the pH_i of K562 and K562/DOX cells treated with cariporide returned to the similar value of the primary levels (Fig. 1B). The pH_i of K562 and K562/DOX cells treated with "high K^+" buffer of different K^+ concentration for 1 and 3 h were induced to 7.2, 7.0 and 6.8 in a few minutes and changed little in the following time. After 48 h recovery in normal culture condition, the pH_i of K562 and K562/DOX cells treated with the "high K^+" buffer also returned to the similar value of the primary levels (Fig. 1C and D). These data suggested that the pH_i of the resistant K562/DOX cells is more alkaline than the sensitive K562 cells. The two kinds of cells could be acidified with cariporide and the "high K^+" buffer method, and the process was reversible.

Decreased pH_i down-regulated the expression of MDR1 mRNA in K562/DOX cells

In K562/DOX cells, cariporide down-regulated MDR1 mRNA expression in a time-dependent manner and the expression were decreased to 74% and 52% of the control after 1 and 3 h treatment. After 48 h recovery in normal culture condition, the MDR1 mRNA expression of K562/DOX cells returned to the similar value of the primary levels (Fig. 2A). The pH_i-effect on MDR1 mRNA was obvious at pH_i 7.2, 7.0 and 6.8 induced by the "high K^+" buffer. The expression was decreased to 84%, 72% and 62% of the control after 1 h treatment and to 71%, 51% and 37% after 3 h treatment. These data indicated that the decrease of MDR1 mRNA expression was also time-dependent. After 48 h recovery in normal culture condition, the MDR1 mRNA expression of K562/DOX cells returned to the similar value of the primary levels (Fig. 2B and C). Nevertheless, these data indicated that the sustained intracellular acidification down-regulated P-gp at mRNA level and the process was reversible.

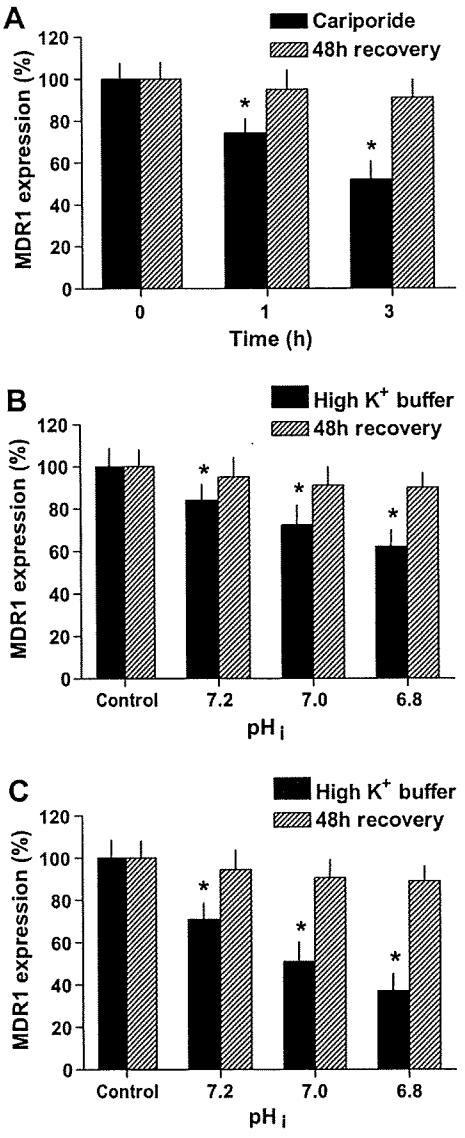

Fig. 2. Determination of MDR1 mRNA expression in K562/DOX cells. (A) The MDR1 mRNA expression of K562/DOX cells after treated with cariporide for 1 and 3 h, and after 48 h recovery from cariporide treatment. (B) The MDR1 mRNA expression of K562/DOX cells after treated with "high K^+" buffer for 1 h, and after 48 h recovery from "high K^+" buffer treatment. (C) The MDR1 mRNA expression of K562/DOX cells after treated with "high K^+" buffer for 3 h, and after 48 h recovery from "high K^+" buffer treatment. Data represent means ± SD of results obtained from three different experiments performed in triplicate. Asterisks indicate statistical significance (p value <0.05, Student's *t*-test).

Please cite this article in press as: Y. Lu et al., Down-regulation of P-glycoprotein expression by sustained intracellular ..., Biochem. Biophys. Res. Commun. (2008), doi:10.1016/j.bbrc.2008.10.005

Decreased pH_i down-regulated P-gp expression in K562/DOX cells

In K562/DOX cells, cariporide down-regulated P-gp expression in a time-dependent manner and the expression were decreased to 78% and 60% of the control after 1 and 3 h treatment as determined by densitometry analysis (Fig. 3A1). After 48 h recovery in normal culture condition, the P-gp expression of K562/DOX cells returned to the similar value of the primary levels (Fig. 3A2). The pH_i-effect on P-gp expression was remarkable at pH_i 7.2, 7.0 and 6.8 induced by the "high K^+" buffer, and the P-gp expression was decreased to 87%, 76% and 64% of the control after 1 h treatment (Fig. 3B1), and to 78%, 58% and 42% after 3 h treatment (Fig. 3C1). After 48 h recovery in normal culture condition, the P-gp expression of K562/DOX cells returned to the similar value of the primary levels (Fig. 3B2 and C2). These data suggested that the sustained intracellular acidification down-regulated P-gp expression also in a pH_i and time-dependent manner, which was in accordance with the results of MDR mRNA expression, and this process was also reversible in K562/DOX cells.

Intracellular acidification enhanced the Rh123 and doxorubicin accumulation in K562/DOX cells

The Rh123 effectively accumulated in K562 cells and was not affected by cariporide and the "high K^+" buffer treatment. The Rh123 accumulation was increased by 3.5-fold compared to the control after cariporide treatment, and by 2.2-, 3.2- and 4.0-fold at pH_i 7.2, 7.0 and 6.8 after the "high K^+" buffer treatment in K562/DOX cells. When K562/DOX cells were pretreated with verapamil, the inhibitor of P-gp, no obvious change of Rh123 accumulation was observed by cariporide and the "high K^+" buffer treatment (Fig. 4A). The accumulation of doxorubicin was much less in the K562/DOX cells compared with the K562 cells. The accumulation was not influenced by cariporide or the "high K^+" buffer in K562 cells, but in K562/DOX cells, it was obviously increased in a pH_i-dependent manner when the cells were pretreated with cariporide and the "high K^+" buffer. The increased doxorubicin distribution into K562/DOX cells nucleus was also observed after the treatment, which might enhance the therapy effect of this drug, as doxorubicin was applied by binding to tumor cells DNA and inhibiting the synthesis of nucleic acid (Fig. 4B). These results suggested that the transport activity of P-gp was down-regulated and the sensitivity of the tumor cells to the chemotherapeutic drug was increased by the sustained intracellular acidification in K562/DOX cells.

Discussion

Chemotherapy as the most potent tools in contemporary medicine has been endangered by the resistance of tumor cells to chemotherapeutical agents. The alkaline pH_i of many and possibly all kinds of malignant cells is known to decrease the retention of anticancer drugs [13–16]. A failure to induce cytosolic acidification has been proposed to be the main factor underlying drug resistance in both the highly alkaline cancer cells and in malignant cells with slightly elevated pH_i [13,17]. It was reported that the pH_i

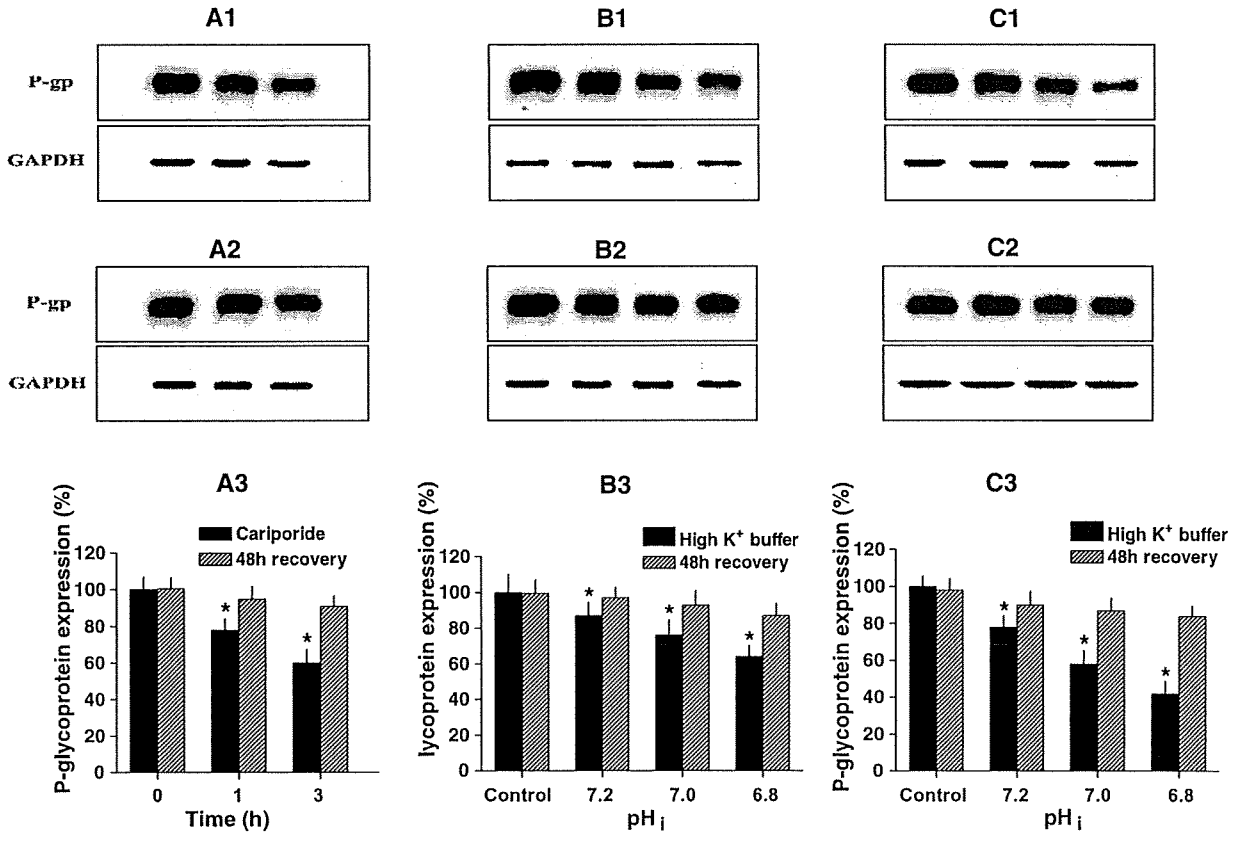

Fig. 3. Determination of P-gp expression in K562/DOX cells. The P-gp expression of K562/DOX cells treated with cariporide for 1 and 3 h (A1) and with "high K^+" buffer for 1 h (B1) and 3 h (C1). The P-gp expression of K562/DOX cells after 48 h recovery from cariporide treatment for 1 and 3 h (A2), and from "high K^+" buffer treatment for 1 h (B2) and 3 h (C2). The intensity of P-gp expression of K562/DOX cells treated with cariporide for 1 and 3 h (A3) and with "high K^+" buffer for 1 h (B3) and 3 h (C3).The intensity of P-gp was quantified by densitometric analysis of the Western blot bands. Data represent means ± SD of results obtained from three different experiments performed in triplicate. Asterisks indicate statistical significance (p value <0.05, Student's t-test).

Please cite this article in press as: Y. Lu et al., Down-regulation of P-glycoprotein expression by sustained intracellular ..., Biochem. Biophys. Res. Commun. (2008), doi:10.1016/j.bbrc.2008.10.005

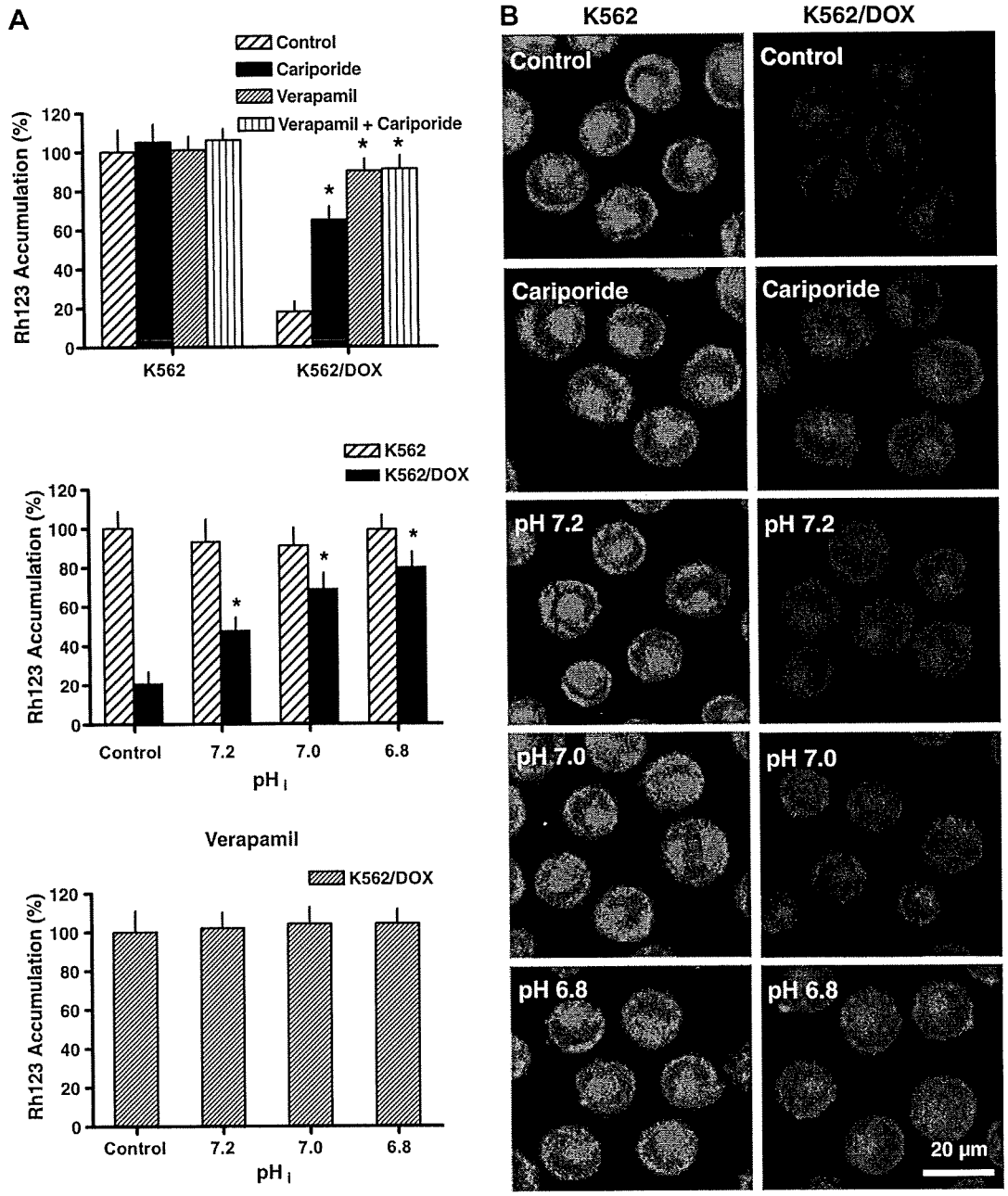

Fig. 4. Effect of sustained intracellular acidification on Rh123 and doxorubicin accumulation in K562 and K562/DOX cells. (A) Rh123 accumulation in K562 and K562/DOX cells treated with cariporide for 3 h, and pretreated with verapamil for 30 min before the cariporide treatment (top). Rh123 accumulation in K562 and K562/DOX cells treated with "high K^+" buffer for 3 h (middle). Rh123 accumulation in K562/DOX cells pretreated with verapamil 50 μmol/l before the "high K^+" buffer treatment (bottom). (B) After the K562 and K562/DOX were treated with cariporide, and the pH_i were induced to 7.2, 7.0, 6.8 with the "high K^+" buffer treatment for 3 h, respectively, the doxorubicin was added to the medium 1 h prior to viewing with confocal laser microscope (500×) as described under Materials and methods. Data represent means ± SD of results obtained from three different experiments performed in triplicate. Asterisks indicate statistical significance (p value <0.05, Student's t-test).

was significantly higher in doxorubicin-resistant human colon carcinoma cells HT29-dx than sensitive HT29 cells, and HT29-dx cells accumulated less doxorubicin than HT29 cells [18]. Similar results have been reached by other groups: with doxorubicin and daunomycin in myeloma [19], adriamycin in the more alkaline MCF-7 human breast cancer cells [20].

The data showed that K562/DOX cells had more alkaline pH_i than K562 cells. The pH_i 7.46 of K562/DOX cells was obviously higher than pH_i 7.1 of K562 cells. The pH_i of the two kinds of cells were induced to about 7.0 by cariporide, and 7.2, 7.0, and 6.8 by "high K^+" buffer. Sustained intracellular acidification increased the accumulation of Rh123 in a pH_i-dependent manner in the K562/DOX cells, but had no effect on the K562 cells. In contrast to these results, intracellular acidification had no apparent effect on Rh123 accumulation in K562/DOX cells pretreated with P-gp inhibitor verapamil, which implied the intracellular acidification might influence the Rh123 kinetics through regulating P-gp activity. The sustained intracellular acidification also increased the doxorubicin accumulation in K562/DOX cells together with the change of doxorubicin distribution, but had no effect on K562 cells. The Fig. 4B showed the increased doxorubicin distribution into the cell nucleus, which might enhance the therapy effect of this drug. The K562/DOX cells

Please cite this article in press as: Y. Lu et al., Down-regulation of P-glycoprotein expression by sustained intracellular ..., Biochem. Biophys. Res. Commun. (2008), doi:10.1016/j.bbrc.2008.10.005

are known to over-express P-gp, but the K562 cells are not. The ability of sustained intracellular acidification to affect Rh123 and doxorubicin kinetics supports the conclusion that the sustained intracellular acidification acts by interfering with a process associated with the P-gp activity. It might occur primarily at the MDR1 mRNA and P-gp expression levels. The data showed that sustained intracellular acidification decreased the MDR1 mRNA expression in a time and pH_i-dependent manner by real-time RT-PCR analysis. Furthermore, over-expression of P-gp in K562/DOX cells was effectively inhibited by the intracellular acidification. The densitometry analysis showed that the expression of P-gp was decreased also in a pH_i and time-dependent manner. The sustained intracellular acidification might affect the expression of MDR1 mRNA and then result in the decreased expression of P-gp, and finally reduce the activity of this membrane protein. After 48 h recovery with the cells pH_i returning to the primary value, the expression of MDR1 mRNA and P-gp were also reverted to the primary levels. The results indicated that the regulative effect of the sustained intracellular acidification on P-gp was reversible, which proved the direct correlation between pH_i and P-gp.

Although the molecular pathways of the regulation of P-gp by pH_i have not been elucidated yet, it was reported that inhibition of the p38-MAPK pathway down-regulated P-gp expression level and diminished the cellular multidrug resistance [21]. SB203580, a specific inhibitor of p38-MAPK pathway, significantly reduced the degree of the vincristine resistance in L1210/VCR cells [22]. Interestingly, it was also reported that NHE1 played a central role in the regulation of MAPK activity [23]. A specific NHE1 inhibitor BIIB722 prevented p38-MAPK phosphorylation, and strongly attenuated apoptosis in cardiomyocytes [24]. And the mechanism of intracellular acidification-induced down-regulation of P-gp activity might be through p38-MAPK pathway, although alternative possible mechanisms may exist.

The available data indicate that any mechanism that leads to an elevation of pH_i might contribute to the onset and maintenance of tumor MDR. Treating malignant diseases along with MDR in the unmodified conditions may continue to limit the therapy success, if efforts are not made to induce intracellular acidification. Therefore, future studies are needed to investigate the specific molecular mechanisms of the regulation of P-gp by pH_i, and the cellular pH_i deserves to be analyzed as a possible important influence factor on the MDR status of tumor cells to the chemotherapy.

Acknowledgment

This work was supported by a grant from General Program of the National Natural Science Foundation of China (No.30570358), Programs of Chinese Ministry of Personnel Foundation for Returned Overseas Chinese Senior Scholars (2005), and the Key Program of Science and Technology Commission Foundation of Tianjin China (No.08JCZDJC19100).

References

[1] J.M. Nørgaard, P. Hokland, Biology of multiple drug resistance in acute leukemia, Int. J. Hematol. 72 (2000) 290–297.
[2] F.H. Labeed, H.M. Coley, H. Thomas, M.P. Hughes, Assessment of multidrug resistance reversal using dielectrophoresis and flow cytometry, Biophys. J. 85 (2003) 2028–2034.
[3] N. Perek, D. Denoyer, F. Dubois, F. Koumanov, Malignant gliomas display altered plasma membrane potential and pH regulation-interaction with Tc-99m-MIBI and Tc-99m-Tetrofosmin uptakes, Gen. Physiol. Biophys. 21 (2002) 381–404.
[4] I.N. Rich, D. Worthington-White, O.A. Garden, P. Musk, Apoptosis of leukemic cells accompanies reduction in intracellular pH after targeted inhibition of the Na^+/H^+ exchanger, Blood 95 (2000) 1427–1434.
[5] P. Wong, H.W. Kleemann, I.F. Tannock, Cytostatic potential of novel agents that inhibit the regulation of intracellular pH, Br. J. Cancer 87 (2002) 238–245.
[6] R.J. Gillies, The tumour microenvironment: causes and consequences of hypoxia and acidity. Introduction, Novartis Found. Symp. 240 (2001) 1–6.
[7] S.J. Reshkin, A. Bellizzi, S. Caldeira, V. Albarani, I. Malanchi, M. Poignee, M. Alunni-Fabbroni, V. Casavola, M. Tommasino, Na^+/H^+ exchanger-dependent intracellular alkalinization is an early event in malignant transformation and plays an essential role in the development of subsequent transformation-associated phenotypes, FASEB J. 14 (2000) 2185–2197.
[8] S. Harguindey, G. Orive, J.L. Pedraz, A. Paradiso, S.J. Reshkin, The role of pH dynamics and the Na^+/H^+ antiporter in the etiopathogenesis and treatment of cancer. Two faces of the same coin–one single nature, Biochim. Biophys. Acta. 1756 (2005) 1–24.
[9] H.J. Rupprecht, J. vom Dahl, W. Terres, K.M. Seyfarth, G. Richardt, H.P. Schultheibeta, M. Buerke, F.H. Sheehan, H. Drexler, Cardioprotective effects of the $Na^{(+)}/H^{(+)}$ exchange inhibitor cariporide in patients with acute anterior myocardial infarction undergoing direct PTCA, Circulation 101 (2000) 2902–2908.
[10] T. Pang, X. Su, S. Wakabayashi, M. Shigekawa, Calcineurin homologous protein as an essential cofactor for Na^+/H^+ exchangers, J. Biol. Chem. 276 (2001) 17367–17372.
[11] S. Wakabayashi, T. Hisamitsu, T. Pang, M. Shigekawa, Mutations of Arg^{440} and Gly^{455}/Gly^{456} oppositely change pH sensing of Na^+/H^+ exchanger 1, J. Biol. Chem. 278 (2003) 11828–11835.
[12] P. Ozkan, R. Mutharasan, A rapid method for measuring intracellular pH using BCECF-AM, Biochim. Biophys. Acta 1572 (2002) 143–148.
[13] Q. Chau, D.J. Stewart, Cisplatin efflux, binding and intracellular pH in the HTB56 human lung adenocarcinoma cell line and the E-8/0.7 cisplatin-resistant variant, Cancer Chemother. Pharmacol. 44 (1999) 193–202.
[14] D. D'Arcangelo, F. Facchiano, L.M. Barlucchi, G. Melillo, B. Illi, L. Testolin, C. Gaetano, M.C. Capogrossi, Acidosis inhibits endothelial cell apoptosis and function and induces basic fibroblast growth factor and vascular endothelial growth factor expression, Circ. Res. 86 (2000) 312–318.
[15] I.J. Fidler, L.M. Ellis, The implications of angiogenesis for the biology and therapy of tumor metastasis, Cell 79 (1994) 185–188.
[16] J.F. Goossens, J.P. Hénichart, L. Dassonneville, M. Facompré, C. Bailly, Relation between intracellular acidification and camptothecin-induced apoptosis in leukemia cells, Eur. J. Pharm. Sci. 10 (2000) 125–131.
[17] S.D. Webb, J.A. Sherratt, R.G. Fish, Mathematical modelling of tumor acidity: regulation of intracellular pH, J. Theor. Biol. 196 (1999) 237–250.
[18] E. Miraglia, D. Viarisio, C. Riganti, C. Costamagna, D. Ghigo, A. Bosia, Na^+/H^+ exchanger activity is increased in doxorubicin-resistant human colon cancer cells and its modulation modifies the sensitivity of the cells to doxorubicin, Int. J. Cancer 115 (2005) 924–929.
[19] S. Simon, D. Roy, M. Schindler, Intracellular pH and the control of multidrug resistance, Proc. Natl. Acad. Sci. USA 91 (1994) 1128–1132.
[20] T. Torigoe, H. Izumi, T. Ise, T. Murakami, H. Uramoto, H. Ishiguchi, Y. Yoshida, M. Tanabe, M. Nomoto, K. Kohno, Vacuolar H^+-ATPase: functional mechanisms and potential as a target for cancer chemotherapy, Anticancer Drugs 13 (2002) 237–243.
[21] K. Katayama, S. Yoshioka, S. Tsukahara, J. Mitsuhashi, Y. Sugimoto, Inhibition of the mitogen-activated protein kinase pathway results in the down-regulation of P-glycoprotein, Mol. Cancer Ther. 6 (2007) 2092–2102.
[22] M. Barancík, V. Bohácová, J. Kvackajová, S. Hudecová, O. Krizanová, A. Breier, SB203580, a specific inhibitor of p38-MAPK pathway, is a new reversal agent of P-glycoprotein-mediated multidrug resistance, Eur. J. Pharm. Sci. 14 (2001) 29–36.
[23] S.F. Pedersen, B.V. Darborg, M.L. Rentsch, M. Rasmussen, Regulation of mitogen-activated protein kinase pathways by the plasma membrane Na^+/H^+ exchanger, NHE1, Arch. Biochem. Biophys. 462 (2007) 195–201.
[24] S. Aker, A.K. Snabaitis, I. Konietzka, A. Van De Sand, K. Böngler, M. Avkiran, G. Heusch, R. Schulz, Inhibition of the Na^+/H^+ exchanger attenuates the deterioration of ventricular function during pacing-induced heart failure in rabbits, Cardiovasc. Res. 63 (2004) 273–282.

Please cite this article in press as: Y. Lu et al., Down-regulation of P-glycoprotein expression by sustained intracellular ..., Biochem. Biophys. Res. Commun. (2008), doi:10.1016/j.bbrc.2008.10.005

Inhibition of Plasminogen Activator Inhibitor-1
Its Mechanism and Effectiveness on Coagulation and Fibrosis

Yuko Izuhara, Satoru Takahashi, Masaomi Nangaku, Shunya Takizawa, Hideyuki Ishida, Kiyoshi Kurokawa, Charles van Ypersele de Strihou, Noriaki Hirayama, Toshio Miyata

Objective—Serine protease inhibitors (serpin) play a central role in various pathological processes including coagulation, fibrinolysis, malignancy, and inflammation. Inhibition of serpins may prove therapeutic. As yet, however, only very few small molecule serpin inhibitors have been reported. For the first time, we apply a new approach of virtual screening to discover novel, orally active, small molecule serpin inhibitors and report their effectiveness.

Methods and Results—We focused on a clinically important serpin, plasminogen activator inhibitor-1 (PAI-1), whose crystal structure has been described. We identify novel, orally active molecules able to enter into the strand 4 position (s4A) of the A β-sheet of PAI-I as a mock compound. In vitro they specifically inhibit the PAI-1 activity and enhance fibrinolysis activity. In vivo the most effective molecule (TM5007) inhibits coagulation in 2 models: a rat arteriovenous (AV) shunt model and a mouse model of ferric chloride–induced testicular artery thrombosis. It also prevents the fibrotic process initiated by bleomycin in mouse lung.

Conclusions—The present study demonstrates beneficial in vitro and in vivo effects of novel PAI-1 inhibitors. Our methodology proves to be a useful tool to obtain effective inhibitors of serpin activity. (***Arterioscler Thromb Vasc Biol.* 2008;28:672-677**)

Key Words: serpin ■ virtual screening ■ anticoagulation ■ antifibrosis ■ plasminogen activator inhibitor-1 inhibitor

Serine protease inhibitors (serpin) play a central role in the regulation of a variety of pathological processes including coagulation, fibrinolysis, malignancy, and inflammation.[1] Their inhibition may prove therapeutic.

Serpins consist of a β-sheets-rich body. They contain an exposed mobile reactive center loop (RCL)[2] which, once cleaved by a target serine protease, inserts its N terminus part into the strand 4 position (s4A) of the A β-sheet, triggering its antiprotease activity. Small molecule compounds able to enter into the s4A position of the A β-sheet as a mock molecule may thus prevent the biological activity of the serpin.

Up to now, however, only very few small molecule serpin inhibitors have been described, none of which are in clinical use. Most have been discovered by high-throughput random screening (HTS) of a large chemical library,[3–5] a rather inefficient strategy. In the present study, a new approach of virtual screening based on the 3-dimensional structure of a serpin, (PAI-1), was used to discover novel, orally active, small molecule compounds able to inhibit the target molecule.

PAI-1 regulates the plasminogen activation system through inhibition of its target serine proteases, tissue-type and urokinase-type plasminogen activator (tPA and uPA).[1] Studies in humans and animals have demonstrated that PAI-1 expression is enhanced in various disorders such as thrombosis, fibrotic diseases, atherosclerosis, radiation damage, and cancer progression.[6] PAI-1 has been linked with fibrin deposition evolving into organ fibrosis and atherosclerosis, or with striking alterations of cell adhesion and migration mediating cancer progression.[7] The absence of PAI-1 in PAI-1 knockout mice markedly attenuates these pathological processes.[8–12] Inhibition of PAI-1 by a neutralizing antibody[13] provides similar promising results in animal experiments. Small molecule PAI-1 inhibitors, active orally, should prove useful to treat not only thrombotic disorders but also fibrotic processes and cancer.[2,14] They should be more efficient than the thrombolytic agents in present use such as streptokinase and recombinant tPA, both of which are protein-based and require intravenous administration to obtain a rapid onset action.

Original received October 8, 2007; final version accepted January 10, 2008.

From the Institute of Medical Sciences (Y.I., K.K., T.M.), Tokai University, Kanagawa, Japan; the Department of Pathology (S.T.), University of Tsukuba School of Medicine, Tsukuba, Japan; the Division of Nephrology and Endocrinology (M.N.), University of Tokyo School of Medicine, Tokyo, Japan; the Divisions of Neurology (S.T.), Physiology (H.I.), and Basic Medical Science and Molecular Medicine (N.H.), Tokai University School of Medicine, Kanagawa, Japan; the Service de Nephrologie (C.v.Y.d.S.), Universite Catholique de Louvain, Brussels, Belgium; and the Division of Translational Medicine (T.M.), Center for Translational and Advanced Animal Research on Human Disease, Tohoku University School of Medicine, Japan.

Correspondence to Toshio Miyata, MD, PhD, Division of Translational Medicine, Center for Translational and Advanced Animal Research on Human Disease, Tohoku University School of Medicine, 2-1 Seiryo-Machi, Aoba-ku, Sendai, 980-8575, Japan. E-mail t-miyata@mail.tains.tohoku.ac.jp

Arterioscler Thromb Vasc Biol **is available at http://atvb.ahajournals.org** **DOI: 10.1161/ATVBAHA.107.157479**

We relied on the 3-dimensional structure of PAI-1 and on the virtual screening method to identify novel orally bioavailable molecules able to fit into the s4A position of PAI-1 as a mock compound. These compounds inhibit PAI-1 activity in vitro and coagulation in vivo in two rodent models of vascular thrombosis. Furthermore, we demonstrate for the first time that they also prevent the fibrotic process induced in mice lung by bleomycin, and thus that, in this model, PAI-1 is not a surrogate marker of fibrosis but rather its main cause.

Materials and Methods

Virtual Screening

Virtual screening was performed by the software system MOE (Molecular Operating Environment).[15] The initial chemical library, of about 2 240 000 entries, merges various commercially available chemicals and deletes redundant entries. In the first step, 2 different filters based on molecular descriptors were used for coarse screening of compounds. The first filter was calculated from drug molecules that are clinically used in Japan. It was represented by the specific distributions of the molecular descriptors for these molecules and represents their general drug-likeness. The second filter was calculated from distributions of the molecular descriptors common to known reference inhibitors[16] and from the inhibitory reactive-center loop peptide N-Ac-TVASS-NH_2[17] that binds PAI-1. It represents the specific lead-likeness of the inhibitory molecules. Through the 2 filters we efficiently reduced the number of compounds to about 3000.[18] The second step involved docking simulation of the selected compounds to the PAI-1 molecule by the program Ph4Dock.[19] The crystal structure (1A7C) of the complex between PAI-1 and the inhibitory reactive-center loop peptide was obtained from the Protein Data Bank[20] and used as the target structure for the docking study. After removal of water molecules and binding peptide, hydrogen atoms were added in accord with the standard protonation states of acidic and basic residues in proteins and their positions were optimized. Because the cleft that is occupied by β-strand 4A in the latent form of PAI-1 likely plays a critical functional role, we focused on it for docking simulation. This target site was characterized by the alpha site finder function[21] in MOE for the subsequent docking experiments. The MMFF94s[22] force field was used in the docking simulation. In the final step, the positions of hydrogen atoms in PAI-1 and all atoms in small molecules were optimized. Docking results were sorted by the following interaction energy.

$$U_{total}=U_{ele}+U_{vdw}+U_{ligand}$$

U_{ele} and U_{vdw} are the electrostatic and van der Waals interactions between the protein and the small molecule, respectively, and U_{ligand} is the conformation energy of the small molecule. The molecules with the lowest U_{total} values are considered as candidate molecules for biological assay.

In Vitro Assays, Toxicity, and Pharmacokinetics

Please see the supplemental data section, available online at http://atvb.ahajournals.org, for detailed Methods.

Arteriovenous Shunt Model

Animal experiments were performed in accordance with the Animal Experimentation Guidelines of Tokai University School of Medicine. Thrombus formation in arteriovenous (AV) shunts was achieved in male CD rats (Charles River Japan Inc, Kanagawa, Japan) by a previously described method.[23] Before the study, TM5007 (300 mg/kg), warfarin (1.2 mg/kg), or ticlopidine (500 mg/kg), suspended in 0.5% carboxymethyl cellulose sodium salt (CMC) solution, was given by gavage, or tPA (275000 IU/kg) was administered intravenously by a bolus injection (n=7 for each group). Control rats were given 0.5% CMC solution only (n=7). Blood was allowed to circulate through the shunt for 30 min. The wet weight of the thrombus covering the silk thread was eventually measured.

Ferric Chloride–Induced Thrombosis Model and Visualization of Thrombi

Male mice were anesthetized with an intraperitoneal injection of 12 mL/kg ketamine-xylazine. Rhodamine 6G (Sigma; 0.1 mL of 0.1%) was injected intravenously. A testicular artery (100 to 150 μm in diameter) was carefully exposed for ferric chloride ($FeCl_3$) treatment. A cotton thread (0.2 mm in diameter) saturated with 0.25 mol/L $FeCl_3$ was applied to the adventitial surface of the testicular artery. After 5 minutes, the cotton thread was replaced by a saline solution in the wound. Thrombus formation in the testicular artery was subsequently monitored through 3-dimensional imaging using an ultrafast laser confocal microscope equipped with a piezo-electric motor control unit as previously reported.[24] The time from endothelial damage by $FeCl_3$ to occlusion of testicular arteries by large thrombi was measured. Mice were pretreated either by gavage of TM5007 (200 mg/kg), twice a day for 4 days. The antiplatelet glycoprotein (GP) IIb/IIIa agent, tirofiban (0.13 mg/kg, Wako), was single administered in a single intravenous injection before the injury.

Bleomycin-Induced Pulmonary Fibrosis

Male C57BL/6J (CLEA Japan Inc.) mice weighing 19 to 21 g were anesthetized with intraperitoneal pentobarbital and their trachea exposed by a cervical incision. Ten animals served as controls. Ten animals received an intratracheal instillation of bleomycin (Nippon Kayaku) dissolved in saline (1.5 U/kg), and 10 animals received in addition by gavage TM5007 (200 mg/kg) suspended in 0.5% CMC, twice a day for 14 days. Lung tissue was obtained for histological analysis and measurement of hydroxyproline content. Hydroxyproline was measured in tissue hydrolysates by the method of Kivirikko et al.[25] Tissue sections were stained with hematoxylin and eosin and pulmonary fibrosis was scored on a scale of 0 to 8 using a previously described method.[26] Azan stain for collagen was also used.

Statistics

All data are expressed as the mean±SE. Differences among groups were assessed by Kruskal-Wallis test. The statistical significance was determined by 2-tailed Mann Whitney U test. Values are considered significant at $P<0.05$. All statistical analyses were performed on the statistical package SPSS for Windows (Version 14.0, SPSS).

Results

Virtual Screening

Our library, encompassing 2 240 000 chemicals, was virtually screened, as described in methods. The use of 2 different filters reduced the number of compounds to about 3000, the first filter assessing drug-likeness and the second evaluating specific lead-likeness of the inhibitory molecules.

Docking simulation was then undertaken by a program Ph4Dock[19] for the remaining compounds. The crystal structure (1A7C) of the complex of PAI-1 with its inhibitory RCL peptide[20] was used, knowing that the 14-aa peptide corresponding to the N terminus of the RCL of PAI-1 inhibits the in vitro activity of PAI-1.[27] The program evaluated whether the compound is able to fit within the PAI-1 cleft. Virtual screening by a combination of 2 filters and by the docking method identified 95 candidate compounds with high binding affinity to the s4A position of PAI-1. The simulated binding mode of 1 novel candidate compound (TM5001) is illustrated (please see supplemental Figure I). The compound binds tightly within the cleft, in the s4A position.

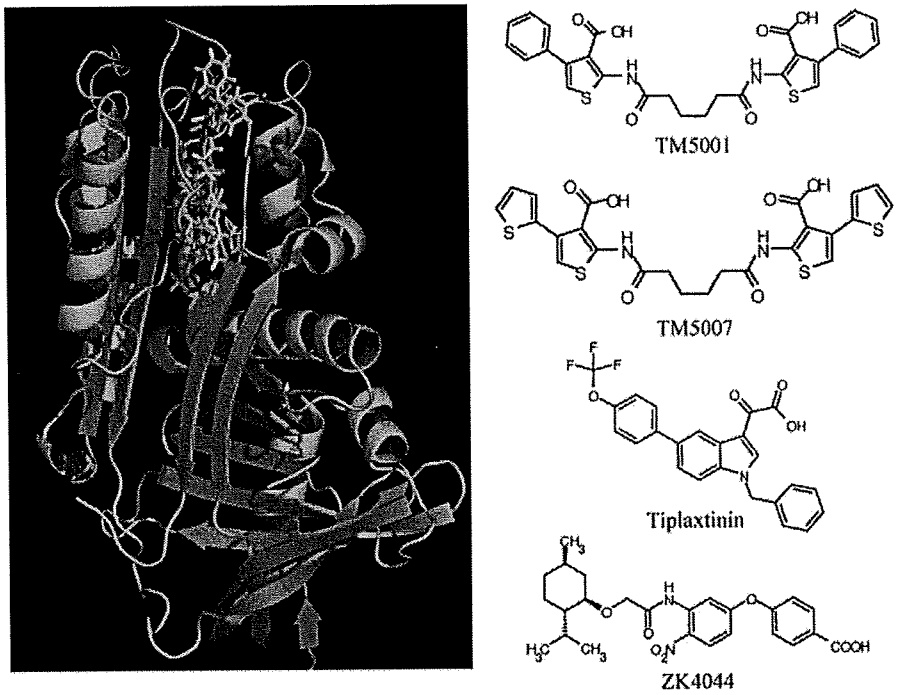

Figure 1. The docking study of small molecules to PAI-1. The binding modes of TM5001 (yellow), TM5007 (red), tiplaxtinin[3] (blue), and ZK4044[5] (green) are shown. Chemical structures of PAI-1 inhibitors are shown. Figures were drawn by a software PyMOL version 0.97 (DeLano Scientific LLC).

Docking simulations were also undertaken for PAI-1 inhibitors previously identified by HTS[3,5] to understand their mechanism of action. Both tiplaxtinin and ZK4044 bind at almost the same site as TM5001 and TM5007 (Figure 1). The similarity of these characteristics suggests that the 4 inhibitors share a common binding region at the s4A position, despite completely different chemical structures.

In Vitro Assessment

We purchased or synthesized 28 of the candidate compounds discovered by virtual screening and tested their biological activities in vitro by three different assays. Inhibition of PAI-1 activity was measured by tPA-dependent hydrolysis of peptide substrate. The 2 most effective candidate compounds, N, N′-bis (3,3′-carboxy-4,4′-phenyl-2,2′-thienyl) hexanedicarboxamide (TM5001) and N, N′-bis [3,3′-carboxy-4,4′-(2,2′-thienyl)-2,2′- thienyl] hexanedicarboxamide (TM5007) had an efficacy comparable to that of tiplaxtinin (IC_{50} for TM5001, TM5007, and tiplaxtinin 28.6±7.3, 29.2±4.2, and 40±7 μmol/L, respectively). TM5001 and TM5007 share a common binding mode with TM5001 as illustrated in Figure 1. It suggests a similar molecular mechanism for their activity. Neither TM5001 nor TM5007 (up to 250 μmol/L) modified other serpin/serine protease systems (ie, α_1-antitrypsin/trypsin and α_2-antiplasmin/plasmin): their PAI-1 inhibitory activity appears thus specific (please see supplemental Figure II).

On SDS-PAGE, PAI-1 formed a covalent complex with tPA whereas no PAI-1/tPA complex formation was observed when PAI-1 was preincubated with our compounds (exemplified for TM5007 in Figure 2).

Finally the inhibition of fibrinolysis was tested on a fibrin plate (exemplified for TM5007). The area of tPA-induced fibrinolysis was decreased by PAI-1. Preincubation of PAI-1 with our compounds prevented this effect (please see supplemental Figure III).

Toxicity and Pharmacokinetics

Cytotoxicity of TM5001 and TM5007 was assessed with HeLa cells as the LDH activity released into the culture medium after 24-h incubation. Results are expressed as percentage of the LDH release induced by the lysis of all cells. TM5001 (100 μmol/L) and TM5007 (250 μmol/L) did

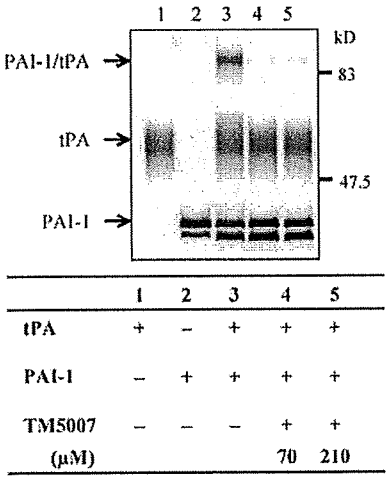

Figure 2. In vitro biological evaluation of PAI-1 inhibitor. The formation of PAI-1/tPA complex was assessed by SDS-PAGE and silver staining.